ISAC Enhancement with Interference Exploitation: From A Uniform Viewpoint for Symbol Level and Block Level

Yiran Wang, Xiaoyan Hu, *Member, IEEE*, Ang Li, *Senior Member, IEEE*, Christos Masouros, *Fellow, IEEE*, Kai-Kit Wong, *Fellow, IEEE*, Kun Yang, *Fellow, IEEE*

***Abstract*—In this paper, we investigate the precoding design based on the concept of constructive interference (CI) for multiple-input multiple-output (MIMO) integrated sensing and communication (ISAC) systems. In particular, we explore the CI-based precoding in both symbol and block levels from a uniform viewpoint, where the radar illumination power is maximized under CI constraint to enhance the sensing performance with guaranteed communication performance. The successive convex approximation (SCA) method is leveraged to effectively solve the formulated non-convex optimization problem. In specific algorithm design, the total power constraint and per-antenna power constraint are considered respectively in order to meet different hardware requirements. Under the total power constraint, we formulate the dual problem of the convex subproblem during SCA processing, which can be efficiently solved by Hooke-Jeeves pattern search algorithm. Under the per-antenna power constraint, we propose a light-weight parallel algorithm based on the alternate direction multiplier method (ADMM). Simulation results show the advantages of the CI-based precoding schemes in enhancing ISAC performance. Under the total power constraint, the proposed CI-based symbol-level precoding (CI-SLP) scheme can achieve satisfactory ISAC performance with low complexity. Under the per-antenna power constraint, the CI-SLP scheme suffers performance loss due to the stringent power constraint, while the performance advantage of the CI-based block-level precoding (CI-BLP) scheme becomes prominent.**

***Index Terms*—Integrated sensing and communication (ISAC), constructive interference (CI), symbol-level precoding (SLP), block-level precoding (BLP).**

I. Introduction

The gradual integration of the physical and digital realms is expected to materialize in the 6G era. This integration spans various applications, from vehicles to drones, from surveillance facilities in cities to agricultural tools in the countryside. To achieve this vision, the wireless industry posits that future networks must possess the ability to sense the physical environment. This sensory capability stands as a unique feature of next-generation networks, moving beyond traditional communication functions. This concept drives researchers to reevaluate the current designs of communication infrastructures and terminals [1]–[3]. Additionally, spectrum resources are becoming increasingly scarce. Spectrum sharing between communication and radar systems is consistent with the idea of building a gradual integration of the physical and digital worlds [4]–[7], which has triggered the recent research area of integrated sensing and communications (ISAC). In this framework, sensing and communication functionalities are possibly jointly designed, optimized, and dispatched to share resources or assist in each other. This integration allows resource sharing and mutual assistance using a single hardware platform, common spectrum, joint signal processing methods, and even a unified control system. However, the differing perspectives regarding the information to be processed in sensing and communication raise several challenges in ISAC systems, particularly for signal processing and waveform design [7].

It is known that there are various kinds of radar and communication performance metrics in ISAC system. In multiple-input multiple-output (MIMO) ISAC systems, the transmit precoding design under different radar and communication performance metrics is the focus of many researchers [8]–[15]. Common radar performance metrics are the signal-to-noise ratio (SNR) of the radar receiver [8], the similarity between the designed and the reference beamformers of radar systems [9]–[11], and the Cramer-Rao bound [12]. At the same time, the widely used communication performance metrics include the multi-user interference (MUI) [13], the signal-to-interference-to-noise ratio (SINR) of communication users [11], and the achievable communication rate [14]. Given the limited system resources, radar performance and communication performance need to be elaborately balanced during the precoding design of ISAC systems under certain metrics, so as to achieve satisfactory system performance.

The precoding designs mentioned above are all conventional block-level precoding (BLP) under the ideal assumption of sufficiently long block length, and their goal is to eliminate inter-user interference. In fact, some existing works have revealed that it is not necessary to completely eliminate inter-user interference in the design of symbol-level precoding (SLP) [16]–[20]. Actually SLP can benefit from interference exploitation and further reduce the error-rate of communication system. The idea of constructive interference (CI) is first mentioned in [16]. The authors of [17] propose a maximum

Y. Wang, X. Hu and A. Li are with the School of Information and Communications Engineering, Faculty of Electronic and Information Engineering, Xian Jiaotong University, Xian, Shaanxi 710049, China (e-mail: yiranwang@stu.xjtu.edu.cn, xiaoyanhu@xjtu.edu.cn, ang.li.2020@xjtu.edu.cn). *(Corresponding author: Xiaoyan Hu.)*

C. Masouros and K.-K. Wong are with the Department of Electronic and Electrical Engineering, University College London, London WC1E 7JE, U.K. (e-mail: c.masouros@ucl.ac.uk, kai-kit.wong@ucl.ac.uk).

K. Yang is with the State Key Laboratory of Novel Software Technology, Nanjing University, Nanjing, 210008, China, and School of Intelligent Software and Engineering, Nanjing University (Suzhou Campus), Suzhou, 215163, China. (e-mail: kunyang@nju.edu.cn).

ratio transmission (MRT) precoding scheme based on strict phase-rotation CI metric. [18] and [19] show that it is enough for the signal to be located in the constructive region. The authors of [20] firstly proposed the symbol-scaling CI metric and therefore extend the exploitation of CI from PSK modulation to QAM modulation. Unlike the conventional BLP, CI-based symbol-level precoding (CI-SLP) individually optimizes the transmit signal in each time slot based on the specific symbols to be sent, rather than simply eliminates the inter-user interference [21]–[23]. From the communication perspective, SLP can exploit CI to reduce the symbol error rate (SER) and perform more reliable multi-user communications. From the radar perspective, the instantaneous transmit beampattern for each sample can be carefully designed and a well-formed beampattern can be guaranteed with a limited number of waveform samples. Hence, the technique of CI-SLP has potentials to enhance the ISAC performance, which has been investigated in recent works [24].

In previous ISAC work [24], the transmit vectors for CI-SLP are optimized to minimize the radar beampattern squared error, subject to CI constraints for communications and power constraints. The simulation results show that the CI-SLP scheme of ISAC system can achieve better instantaneous beampattern and better SER performance than conventional BLP schemes. However, due to the complicated processing of quartic function in the optimization objective and the need for thousands of iterations, the computational complexity of this scheme is too high to be accepted in practical systems. In [25], the authors jointly optimize transmit signals and receive filters for MIMO-ISAC by leveraging space-time adaptive processing (STAP) and CI-SLP. In [26], the authors extend the framework to wideband FTN-ISAC, formulating the corresponding CI-SLP problem under faster-than-Nyquist signaling. A CI-SLP design for OFDM-ISAC is proposed in [27], where the range-Doppler integrated sidelobe level (ISL) of the ambiguity function is minimized while target illumination power, communication CI, and transmit power constraints are satisfied. Building on the ISAC paradigm presented in [24], a deep-learning-based framework is introduced in [28] to enable low-complexity CI-SLP implementation. Nevertheless, this scheme exhibits a modest performance loss compared with the scheme in [24]. In [29], a low-complexity CI-SLP scheme based on communication CI and radar illumination power is proposed. This scheme enhances the ISAC performance while significantly reducing the computational complexity. However, this low-complexity algorithm is only applicable to single-target scenarios under the total power constraint. In this paper, we strive to develop a low-complexity CI-SLP scheme for the multi-target ISAC system, considering more practical power constraints.

Although CI-SLP can bring gains in ISAC performance with instantaneous beampattern design, the symbol-by-symbol optimization requires high real-time processing which may induce significant burden to the signal processing units of system hardware. In addition, the symbol-by-symbol power constraints introduce additional limitations to the optimization problem, thereby causing a certain performance loss, especially under the per-antenna power constraint. In fact, the radar beampattern normally need to be averaged after several samples in practical systems, so it is not necessary to strictly design the instantaneous beampattern for each sample. Recently, the authors in [30] propose a CI-based BLP (CI-BLP) in communication-only system for the first time, which can offer an improved error-rate performance compared with the CI-SLP approaches. Meanwhile, compared with the CI-SLP schemes that optimize the transmit signals at the symbol level, the CI-BLP schemes consider a block of symbols and the optimization requires execution only once for each block of symbol slots, which can greatly reduce the update frequency of the transmit precoders [31]. Moreover, in the ISAC system, the design philosophy and performance metrics of CI-SLP are quite different from those of conventional BLP. Currently, no research has compared symbol-level design and block-level design from a unified perspective, so it remains unknown which one is more suitable for the ISAC system. In this paper, to fully investigate the ISAC performance of SLP and BLP schemes and facilitate the design processing, we try to design the CI-based precoding for ISAC systems in a uniform viewpoint for both symbol level and block level.

In this paper, the design of CI-based precoding for MIMO ISAC systems is investigated, where a multi-antenna ISAC base station (BS) serves multiple single-antenna communication users while simultaneously detecting multiple targets of interest. Specifically, the illumination power of radar is maximized under communication CI constraint. Furthermore, by extending the proposed precoding scheme from symbol level to block level, a unified problem form can be obtained. In the specific algorithm design, we consider the total power constraint and the per-antenna power constraint respectively to better meet different hardware requirements, and the algorithms are separately designed. The main contributions of this paper can be summarized as follows:

1) We propose the CI-based precoding design schemes for the MIMO ISAC systems. Both the CI-SLP and CI-BLP schemes are considered to enhance the ISAC performance. The uniform problem formulations are achieved for both precoding scenarios, under the total and per-antenna power constrains, respectively. Since the optimization objective function is not convex, we leverage the successive convex approximation (SCA) method to effectively solve the proposed optimization problems.
2) For the case of the total power constraint, we analyze the Lagrangian function and Karush-Kuhn-Tucker (KKT) conditions of the convex subproblem obtained through the SCA method, and then formulate the corresponding dual problem. It is easy to prove that the dual problem can be more efficiently solved with Hooke-Jeeves pattern search algorithm.
3) Further considering the hardware requirements, per-antenna power constraints are more preferred in practical ISAC systems. For the case with the per-antenna power constraints, the dual problem of the subproblem is difficult to be expressed. To address this issue, we utilize a simple parallel algorithm [32] and the alternate direction multiplier method (ADMM) [33], which is proved with significantly reduced computational complexity.

4) Simulation results demonstrate that under the total power constraint, the proposed CI-SLP scheme can achieve satisfactory ISAC performance with low complexity. Under the per-antenna power constraint, the CI-SLP scheme suffers performance loss due to the stringent power constraint, while the performance advantage of the CI-BLP scheme becomes prominent. This work also provides a reference for the selection between CI-SLP and CI-BLP in practical systems.

We organize the rest of the paper as follows. The system model, radar model and communication model are introduced in Section II. The proposed CI-SLP and CI-BLP schemes under total power constraint and per-antenna power constrainta are presented in Sections III and IV, respectively. Simulation results are demonstrated in Section V with thorough analysis, and the final conclusions are provided in Section VI.

Notations: In this document, lowercase, bold lowercase, and bold uppercase letters signify scalars, vectors, and matrices, respectively. The symbols $\mathbb{R}$ and $\mathbb{C}$ represent the sets of real and complex numbers. Superscripts $^{\mathrm{T}}$ and $^{\mathrm{H}}$ denote the transpose and the conjugate transpose operations, respectively. The operator $\|\cdot\|_2$ indicates the 2-norm of a vector. The expressions $\Re\{\cdot\}$ and $\Im\{\cdot\}$ extract the real and imaginary components of the input, respectively. We define $\mathbf{I}_N$ as the identity matrix of size $N \times N$. Lastly, $\mathbf{1}$ and $\mathbf{0}$ represent the all-one vector and the all-zero vector, respectively.

II. System Model and Preliminaries

A. System Model

In this paper, a MIMO ISAC system is considered, which transmits a single waveform for both radar probing and communicating data symbols to downlink users simultaneously. The ISAC BS utilizes a uniform linear array (ULA) comprising N antennas, serving K_{u} single-antenna users while detecting K_{t} targets. Typically, conditions hold that $K_{\mathrm{u}} \leq N$ and $K_{\mathrm{t}} \leq N$. The identical antenna array facilitates both transmission and reception through the time-division duplex (TDD) protocol.

The transmit signal matrix $\mathbf{X} = [\mathbf{x}[1], \mathbf{x}[2], \cdots, \mathbf{x}[L]] \in \mathbb{C}^{N\times L}$ is used as the baseband representation of the ISAC waveform for both radar and communication operations, and L represents number of time slots within the considered block which may be shorter than the coherence interval of the channel. In this case, $\mathbf{x}[l] = [x_1[l], x_2[l], \cdots, x_N[l]]^{\mathrm{T}} \in \mathbb{C}^{N\times 1}$ is the corresponding ISAC waveform in the l-th time slot with $l \in \mathcal{L} \triangleq \{1, 2, \cdots, L\}$. The data symbol matrix is $\mathbf{S} = [\mathbf{s}[1], \mathbf{s}[2], \cdots, \mathbf{s}[L]] \in \mathbb{C}^{K_{\mathrm{u}}\times L}$ and the data symbol vector in the l-th time slot is represented as $\mathbf{s}[l] = [s_1[l], s_2[l], \cdots, s_{K_{\mathrm{u}}}[l]]^{\mathrm{T}} \in \mathbb{C}^{K_{\mathrm{u}}\times 1}$, and its elements are selected from a unit-norm PSK constellation. Unlike the conventional BLP designs, the CI-SLP and CI-BLP optimize $\mathbf{x}[l]$ or $\mathbf{X}$ directly according to the instantaneous data symbols $\mathbf{s}[l]$ or $\mathbf{S}$ instead of optimizing the second-order statistic of $\mathbf{X}$.

B. Radar Model

Under the assumption that the transmitted probing signals are narrowband and that the propagation is non-dispersive, the baseband signal at the k_{t}-th target location in the l-th time slot can be represented as

$$r_{k_{\mathrm{t}}}[l] = \mathbf{a}(\theta_{k_{\mathrm{t}}})^{\mathrm{H}} \mathbf{x}[l], \tag{1}$$

where $\mathbf{a}(\theta_{k_{\mathrm{t}}}) = \left[1, e^{j\sin\theta_{k_{\mathrm{t}}}}, \cdots, e^{j(N-1)\sin\theta_{k_{\mathrm{t}}}}\right]^{\mathrm{T}} \in \mathbb{C}^{N\times 1}$ represents the transmit steering vector of the ISAC BS towards the target with $\theta_{k_{\mathrm{t}}}$ as the corresponding azimuth angle.

It follows from (1) that the illumination power [34] of the probing signal $\mathbf{x}[l]$ at the k_{t}-th target location is given by

$$P(\theta_{k_{\mathrm{t}}}) = \mathbf{a}(\theta_{k_{\mathrm{t}}})^{\mathrm{H}} \mathbf{x}[l]\, \mathbf{x}^{\mathrm{H}}[l]\, \mathbf{a}(\theta_{k_{\mathrm{t}}}). \tag{2}$$

By defining $\mathbf{a}_{\mathrm{E},k_{\mathrm{t}}} \in \mathbb{C}^{2N\times 1}$, $\mathbf{b}_{\mathrm{E},k_{\mathrm{t}}} \in \mathbb{C}^{2N\times 1}$ and $\mathbf{x}_{\mathrm{E},l} \in \mathbb{R}^{2N\times 1}$ as follows

$$\mathbf{a}_{\mathrm{E},k_{\mathrm{t}}} = \left[\Re\left(\mathbf{a}^{\mathrm{T}}(\theta_{k_{\mathrm{t}}})\right), \Im\left(\mathbf{a}^{\mathrm{T}}(\theta_{k_{\mathrm{t}}})\right)\right]^{\mathrm{T}}, \tag{3}$$

$$\mathbf{b}_{\mathrm{E},k_{\mathrm{t}}} = \left[-\Im\left(\mathbf{a}^{\mathrm{T}}(\theta_{k_{\mathrm{t}}})\right), \Re\left(\mathbf{a}^{\mathrm{T}}(\theta_{k_{\mathrm{t}}})\right)\right]^{\mathrm{T}}, \tag{4}$$

$$\mathbf{x}_{\mathrm{E},l} = \left[\Re\left(\mathbf{x}^{\mathrm{T}}[l]\right), \Im\left(\mathbf{x}^{\mathrm{T}}[l]\right)\right], \tag{5}$$

the cumulated illumination power of all target locations can be expressed as a standard quadratic form:

$$\begin{aligned} P_{\mathrm{t}} &= \sum_{k_{\mathrm{t}}=1}^{K_{\mathrm{t}}} \mathbf{a}(\theta_{k_{\mathrm{t}}})^{\mathrm{H}} \mathbf{x}[l]\, \mathbf{x}^{\mathrm{H}}[l]\, \mathbf{a}(\theta_{k_{\mathrm{t}}}) \\ &= \sum_{k_{\mathrm{t}}=1}^{K_{\mathrm{t}}} \left|\mathbf{a}_{\mathrm{E},k_{\mathrm{t}}}^{\mathrm{T}} \mathbf{x}_{\mathrm{E},l}\right|^2 + \sum_{k_{\mathrm{t}}=1}^{K_{\mathrm{t}}} \left|\mathbf{b}_{\mathrm{E},k_{\mathrm{t}}}^{\mathrm{T}} \mathbf{x}_{\mathrm{E},l}\right|^2 = \mathbf{x}_{\mathrm{E},l}^{\mathrm{T}} \mathbf{D} \mathbf{x}_{\mathrm{E},l}, \end{aligned} \tag{6}$$

where the matrix $\mathbf{D} \in \mathbb{R}^{2N\times 2N}$ is defined as:

$$\mathbf{D} = \sum_{k_{\mathrm{t}}=1}^{K_{\mathrm{t}}} \mathbf{a}_{\mathrm{E},k_{\mathrm{t}}} \mathbf{a}_{\mathrm{E},k_{\mathrm{t}}}^{\mathrm{T}} + \sum_{k_{\mathrm{t}}=1}^{K_{\mathrm{t}}} \mathbf{b}_{\mathrm{E},k_{\mathrm{t}}} \mathbf{b}_{\mathrm{E},k_{\mathrm{t}}}^{\mathrm{T}}. \tag{7}$$

Note that the radar illumination power towards the target is expected to be as high as possible to ensure the detection probability (DP) of the targets [34], [35]. Therefore, we try to maximize the radar illumination power through optimizing the precoding vector $\mathbf{x}_{\mathrm{E},l}$, which can be expressed as

$$\max_{\mathbf{x}_{\mathrm{E},l}} \ \mathbf{x}_{\mathrm{E},l}^{\mathrm{T}} \mathbf{D} \mathbf{x}_{\mathrm{E},l} \Rightarrow \min_{\mathbf{x}_{\mathrm{E},l}} \ -\mathbf{x}_{\mathrm{E},l}^{\mathrm{T}} \mathbf{D} \mathbf{x}_{\mathrm{E},l}. \tag{8}$$

C. Communication Model

As for communications, the received signal for the k-th user in the l-th time slot can be written as

$$y_k[l] = \mathbf{h}_k^{\mathrm{T}} \mathbf{x}[l] + n_k[l], \tag{9}$$

where $\mathbf{h}_k \in \mathbb{C}^{N\times 1}$ is the channel between BS and the k-th user, remaining constant throughout the considered block. In addition, $n_k[l] \sim \mathcal{CN}(0, \sigma_k^2)$ represents the additive white Gaussian noise (AWGN) at the k-th user in the l-th slot.

In this paper, we adopt the symbol-scaling-based CI metric, which is different from the commonly used phase-rotation-based CI metric and it can be easily extended to QAM modulation [36]. To demonstrate the symbol-scaling CI metric proposed in [23], we display one quarter of a QPSK constellation in Fig. 1 as an example. For brevity, we omit the time slot index $[l]$ in Fig. 1. Without loss of generality, $\overrightarrow{OA}$ represents the nominal constellation point of the k-th user in the l-th slot,

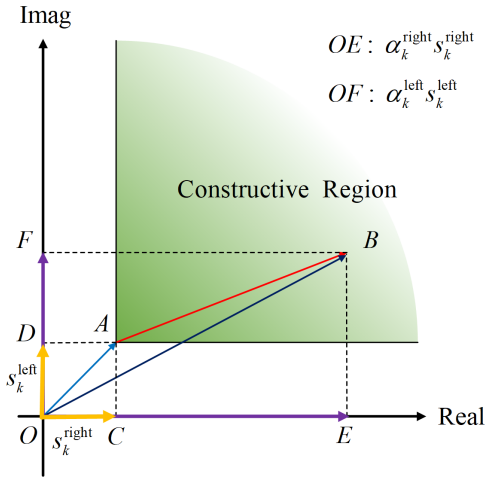

Fig. 1. Geometric diagram of the symbol-scaling CI metric for QPSK.

i.e., $\overrightarrow{OA} = s_k[l]$. $\overrightarrow{OB}$ represents the corresponding noise-free received signal with interference and $\overrightarrow{AB}$ can be considered as the sum of interference. Based on the geometry we obtain

$$\begin{aligned}\overrightarrow{OB} &= \overrightarrow{OA} + \overrightarrow{AB} = \mathbf{h}_k^{\mathrm{T}}\mathbf{x}[l] \\ &= \left[\Re(\mathbf{h}_k)^{\mathrm{T}}\Re(\mathbf{x}[l]) - \Im(\mathbf{h}_k)^{\mathrm{T}}\Im(\mathbf{x}[l])\right] \\ &\quad + j\cdot\left[\Im(\mathbf{h}_k)^{\mathrm{T}}\Re(\mathbf{x}[l]) + \Re(\mathbf{h}_k)^{\mathrm{T}}\Im(\mathbf{x}[l])\right]. \end{aligned} \tag{10}$$

The idea of the symbol-scaling CI metric is that the signal is decomposed along two decision boundaries, and then CI is measured by the scaling factors obtained from the decomposition. To be more specific, in Fig. 1, $\overrightarrow{OA}$ can be decomposed along the two decision boundaries for QPSK modulation as $\overrightarrow{OA} = \overrightarrow{OC} + \overrightarrow{OD} = s_k^{\text{right}}[l] + s_k^{\text{left}}[l]$, where $s_k^{\text{right}}[l]$ and $s_k^{\text{left}}[l]$ represent the projections of the k-th user's nominal constellation point onto the two decision boundaries, respectively. In a similar way, the received signal $\overrightarrow{OB}$ can also be decomposed as follows.

$$\begin{aligned}\overrightarrow{OB} &= \overrightarrow{OE} + \overrightarrow{OF} = \alpha_k^{\text{right}}[l]\, s_k^{\text{right}}[l] + \alpha_k^{\text{left}}[l]\, s_k^{\text{left}}[l] \\ &= \alpha_k^{\text{right}}[l]\left[\Re\left(s_k^{\text{right}}[l]\right) + j\cdot\Im\left(s_k^{\text{right}}[l]\right)\right] \\ &\quad + \alpha_k^{\text{left}}[l]\left[\Re\left(s_k^{\text{left}}[l]\right) + j\cdot\Im\left(s_k^{\text{left}}[l]\right)\right] \\ &= \left[\alpha_k^{\text{right}}[l]\,\Re\left(s_k^{\text{right}}[l]\right) + \alpha_k^{\text{left}}[l]\,\Re\left(s_k^{\text{left}}[l]\right)\right] \\ &\quad + j\cdot\left[\alpha_k^{\text{right}}[l]\,\Im\left(s_k^{\text{right}}[l]\right) + \alpha_k^{\text{left}}[l]\,\Im\left(s_k^{\text{left}}[l]\right)\right], \end{aligned} \tag{11}$$

where $\alpha_k^{\text{right}}[l]$ and $\alpha_k^{\text{left}}[l]$ represent the non-negative scaling factors corresponding to the two decision boundaries, respectively. The real and imaginary parts of $\overrightarrow{OB}$ expressed in (10) and (11) are equal respectively, and thus the following two equations can be obtained:

$$\begin{aligned}&\Re(\mathbf{h}_k)^{\mathrm{T}}\Re(\mathbf{x}[l]) - \Im(\mathbf{h}_k)^{\mathrm{T}}\Im(\mathbf{x}[l]) \\ &\quad = \alpha_k^{\text{right}}[l]\,\Re\left(s_k^{\text{right}}[l]\right) + \alpha_k^{\text{left}}[l]\,\Re\left(s_k^{\text{left}}[l]\right), \\ &\Im(\mathbf{h}_k)^{\mathrm{T}}\Re(\mathbf{x}[l]) + \Re(\mathbf{h}_k)^{\mathrm{T}}\Im(\mathbf{x}[l]) \\ &\quad = \alpha_k^{\text{right}}[l]\,\Im\left(s_k^{\text{right}}[l]\right) + \alpha_k^{\text{left}}[l]\,\Im\left(s_k^{\text{left}}[l]\right). \end{aligned} \tag{12}$$

Through simple mathematical operations from (12), a linear relationship between each scaling factor and the transmit signal can be obtained as:

$$\boldsymbol{\alpha}_{\mathrm{E},l} = \mathbf{M}_l\mathbf{x}_{\mathrm{E},l}, \tag{13}$$

so that each scaling factor can be directly represented by the transmit signal. Here, $\mathbf{x}_{\mathrm{E},l} \in \mathbb{R}^{2N\times 1}$ has been defined in (5). The scaling factors for all users are collected in vector $\boldsymbol{\alpha}_{\mathrm{E},l} \in \mathbb{R}^{2K_{\mathrm{u}}\times 1}$, which is defined as

$$\boldsymbol{\alpha}_{\mathrm{E},l} = \left[\alpha_1^{\text{right}}[l], \cdots, \alpha_{K_{\mathrm{u}}}^{\text{right}}[l], \alpha_1^{\text{left}}[l], \cdots, \alpha_{K_{\mathrm{u}}}^{\text{left}}[l]\right]^{\mathrm{T}}. \tag{14}$$

In addition, the coefficient matrix $\mathbf{M}_l \in \mathbb{R}^{2K_{\mathrm{u}}\times 2N}$ in (13) is constructed as [37]:

$$\mathbf{M}_l = \left[\mathbf{p}_1, \mathbf{p}_2, \cdots, \mathbf{p}_{K_{\mathrm{u}}}, \mathbf{q}_1, \mathbf{q}_2, \cdots, \mathbf{q}_{K_{\mathrm{u}}}\right]^{\mathrm{T}}, \tag{15}$$

where $\mathbf{p}_k \in \mathbb{R}^{2N\times 1}$ and $\mathbf{q}_k \in \mathbb{R}^{2N\times 1}$ are given by

$$\mathbf{p}_k = \begin{bmatrix} \frac{\Im\left(s_k^{\text{left}}[l]\right)\Re(\mathbf{h}_k) - \Re\left(s_k^{\text{left}}[l]\right)\Im(\mathbf{h}_k)}{\Re\left(s_k^{\text{right}}[l]\right)\Im\left(s_k^{\text{left}}[l]\right) - \Im\left(s_k^{\text{right}}[l]\right)\Re\left(s_k^{\text{left}}[l]\right)} \\ -\frac{\Im\left(s_k^{\text{left}}[l]\right)\Im(\mathbf{h}_k) + \Re\left(s_k^{\text{left}}[l]\right)\Re(\mathbf{h}_k)}{\Re\left(s_k^{\text{right}}[l]\right)\Im\left(s_k^{\text{left}}[l]\right) - \Im\left(s_k^{\text{right}}[l]\right)\Re\left(s_k^{\text{left}}[l]\right)} \end{bmatrix}, \tag{16}$$

$$\mathbf{q}_k = \begin{bmatrix} \frac{\Re\left(s_k^{\text{right}}[l]\right)\Im(\mathbf{h}_k) - \Im\left(s_k^{\text{right}}[l]\right)\Re(\mathbf{h}_k)}{\Re\left(s_k^{\text{right}}[l]\right)\Im\left(s_k^{\text{left}}[l]\right) - \Im\left(s_k^{\text{right}}[l]\right)\Re\left(s_k^{\text{left}}[l]\right)} \\ \frac{\Re\left(s_k^{\text{right}}[l]\right)\Re(\mathbf{h}_k) + \Im\left(s_k^{\text{right}}[l]\right)\Im(\mathbf{h}_k)}{\Re\left(s_k^{\text{right}}[l]\right)\Im\left(s_k^{\text{left}}[l]\right) - \Im\left(s_k^{\text{right}}[l]\right)\Re\left(s_k^{\text{left}}[l]\right)} \end{bmatrix}. \tag{17}$$

Referring to Fig. 1, it can be observed that the values of $\alpha_k^{\text{right}}[l]$ and $\alpha_k^{\text{left}}[l]$ reflect the constructive effect. A greater value of either $\alpha_k^{\text{right}}[l]$ or $\alpha_k^{\text{left}}[l]$ indicates that the received symbol moves further away from one of its decision boundaries. This movement facilitates symbol detection, thereby enhancing the communication error-rate performance of ISAC systems. Based on the above description, the communication constraint with symbol-scaling CI metric can be formulated as

$$\boldsymbol{\alpha}_{\mathrm{E},l} = \mathbf{M}_l\mathbf{x}_{\mathrm{E},l} \geq t, \tag{18}$$

where $t = \sigma_{\max}\Gamma$ is the lower bound of all scaling factors and also represents the reliable distance between the constructive region and the corresponding decision boundary. Here, $\sigma_{\max}$ is the maximum value in $\{\sigma_1, \cdots, \sigma_{K_{\mathrm{u}}}\}$, representing the maximum noise power for all users, and Γ is the SINR threshold. Note that the communication CI constraint can be guaranteed through designing the precoding vector $\mathbf{x}_{\mathrm{E},l}$.

III. Precoding Design under Total Power Constraint

In this section, we design the transmit ISAC waveform matrix $\mathbf{X}$ (which is equivalent to design $\mathbf{x}_{\mathrm{E},l}, \forall l \in \mathcal{L}$). The radar illumination power towards targets is maximized under total power constraint, while satisfying the communication constraint with symbol-scaling CI metric. Next, we will formulate the corresponding ISAC waveform design problems with both SLP and BLP protocols and proposed a uniform algorithm to solve the optimization problems.

A. Problem Formulation with CI-SLP

In the l-th time slot, the CI-SLP optimization problem for maximizing the illumination power of the ISAC system under total power constraint can be formulated as

$$\mathcal{P}_1^{\text{CI-SLP-TPC}}: \min_{\mathbf{x}_{\mathrm{E},l}} \ -\mathbf{x}_{\mathrm{E},l}^{\mathrm{T}}\mathbf{D}\mathbf{x}_{\mathrm{E},l} \tag{19}$$

$$\text{s.t.} \ \ \mathbf{M}_l\mathbf{x}_{\mathrm{E},l} \geq t, \tag{19a}$$

$$\|\mathbf{x}_{\mathrm{E},l}\|_2^2 \leq p_0, \tag{19b}$$

where p_0 represents the transmit power budget for the ISAC BS within each symbol slot.

B. Problem Formulation with CI-BLP

For the entire considered block, the CI-BLP optimization problem for maximizing the illumination power of the ISAC system under total power constraint can be formulated as

$$\mathcal{P}_1^{\text{CI-BLP-TPC}}: \min_{\{\mathbf{x}_{\mathrm{E},l}\}} \ -\sum_{l=1}^{L}\mathbf{x}_{\mathrm{E},l}^{\mathrm{T}}\mathbf{D}\mathbf{x}_{\mathrm{E},l} \tag{20}$$

$$\text{s.t.} \ \ \mathbf{M}_l\mathbf{x}_{\mathrm{E},l} \geq t, \forall l \in \mathcal{L}, \tag{20a}$$

$$\sum_{l=1}^{L}\|\mathbf{x}_{\mathrm{E},l}\|_2^2 \leq Lp_0. \tag{20b}$$

In fact, $\mathcal{P}_1^{\text{CI-BLP-TPC}}$ can be equivalently re-expressed more concisely as

$$\mathcal{P}_2^{\text{CI-BLP-TPC}}: \min_{\tilde{\mathbf{x}}_{\mathrm{E}}} \ -\tilde{\mathbf{x}}_{\mathrm{E}}^{\mathrm{T}}\tilde{\mathbf{D}}\tilde{\mathbf{x}}_{\mathrm{E}} \tag{21}$$

$$\text{s.t.} \ \ \tilde{\mathbf{M}}\tilde{\mathbf{x}}_{\mathrm{E}} \geq t, \tag{21a}$$

$$\|\tilde{\mathbf{x}}_{\mathrm{E}}\|_2^2 \leq Lp_0, \tag{21b}$$

where $\tilde{\mathbf{x}}_{\mathrm{E}} \in \mathbb{R}^{2LN\times 1}$, $\tilde{\mathbf{D}} \in \mathbb{R}^{2LN\times 2LN}$ and $\tilde{\mathbf{M}} \in \mathbb{R}^{2LK_{\mathrm{u}}\times 2LN}$ are respectively defined as:

$$\tilde{\mathbf{x}}_{\mathrm{E}} = \left[\mathbf{x}_{\mathrm{E},1}^{\mathrm{T}}, \cdots, \mathbf{x}_{\mathrm{E},L}^{\mathrm{T}}\right]^{\mathrm{T}}, \tag{22}$$

$$\tilde{\mathbf{D}} = \mathbf{I}_L \otimes \mathbf{D}, \quad \tilde{\mathbf{M}} = \mathrm{diag}\left(\mathbf{M}_1, \mathbf{M}_2, \cdots, \mathbf{M}_L\right). \tag{23}$$

Here, $\otimes$ represents the Kronecker product and $\tilde{\mathbf{M}}$ is a block diagonal matrix, with each diagonal block being the coefficient matrix $\mathbf{M}_l$ ($l \in \mathcal{L}$) corresponding to each time slot in the block.

Remark 1: *Obviously, the CI-SLP scheme in each time slot is a special case of the CI-BLP scheme when $L = 1$. Therefore, the subsequent algorithm is designed for CI-BLP which is also applicable to CI-SLP. For the convenience of expression, we simplify $\mathcal{P}_2^{\text{CI-BLP-TPC}}$ as $\mathcal{P}_2^{\text{TPC}}$, which is a general optimization problem form for both the cases of CI-SLP and CI-BLP.*

C. Algorithm Design with SCA Transformation

It is easy to note that the problem $\mathcal{P}_2^{\text{TPC}}$ given in (21) is non-convex because of the concave objective function. In order to effectively solve the non-convex optimization problem $\mathcal{P}_2^{\text{TPC}}$, we adopt the SCA method. First, let us denote the objective function as

$$f\left(\tilde{\mathbf{x}}_{\mathrm{E}}\right) = -\tilde{\mathbf{x}}_{\mathrm{E}}^{\mathrm{T}}\tilde{\mathbf{D}}\tilde{\mathbf{x}}_{\mathrm{E}}, \ \tilde{\mathbf{x}}_{\mathrm{E}} \in \mathcal{Q}_{\mathrm{TPC}}, \tag{24}$$

and we define $\mathcal{Q}_{\mathrm{TPC}}$ as the feasible region of $\mathcal{P}_2^{\text{TPC}}$ constrained by (21a) and (21b), which is a convex set of $\tilde{\mathbf{x}}_{\mathrm{E}}$. In the m-th iteration of the SCA process, the objective function can be approximated by its upper bound achieved from its first-order Taylor expansion near the point obtained in $(m-1)$-th iteration given as $\tilde{\mathbf{x}}_{\mathrm{E}}^{m-1} \in \mathcal{Q}_{\mathrm{TPC}}$. Hence, we have

$$f\left(\tilde{\mathbf{x}}_{\mathrm{E}}\right) \leq f\left(\tilde{\mathbf{x}}_{\mathrm{E}}^{m-1}\right) + \bigtriangledown f\left(\tilde{\mathbf{x}}_{\mathrm{E}}^{m-1}\right)^{\mathrm{T}}\left(\tilde{\mathbf{x}}_{\mathrm{E}} - \tilde{\mathbf{x}}_{\mathrm{E}}^{m-1}\right) \triangleq \hat{f}\left(\tilde{\mathbf{x}}_{\mathrm{E}}\right), \tag{25}$$

where $\bigtriangledown f\left(\cdot\right)$ denotes the gradient of $f\left(\cdot\right)$ versus $\tilde{\mathbf{x}}_{\mathrm{E}}$ and

$$\bigtriangledown f\left(\tilde{\mathbf{x}}_{\mathrm{E}}^{m-1}\right) = -2\tilde{\mathbf{D}}\tilde{\mathbf{x}}_{\mathrm{E}}^{m-1}. \tag{26}$$

Note that only $\bigtriangledown f\left(\tilde{\mathbf{x}}_{\mathrm{E}}^{m-1}\right)^{\mathrm{T}}\tilde{\mathbf{x}}_{\mathrm{E}}$ is related to $\tilde{\mathbf{x}}_{\mathrm{E}}$ in the objective $\hat{f}\left(\tilde{\mathbf{x}}_{\mathrm{E}}\right)$, and the other constant terms in (25) can be ignored. Therefore, we can equivalently solve the following optimization problem at the m-th iteration of the SCA method:

$$\mathcal{P}_3^{\text{TPC}}: \min_{\tilde{\mathbf{x}}_{\mathrm{E}}} \ \mathbf{d}^{\mathrm{T}}\tilde{\mathbf{x}}_{\mathrm{E}} \tag{27}$$

$$\text{s.t.} \ \ \tilde{\mathbf{M}}\tilde{\mathbf{x}}_{\mathrm{E}} \geq t, \tag{27a}$$

$$\|\tilde{\mathbf{x}}_{\mathrm{E}}\|_2^2 \leq Lp_0, \tag{27b}$$

where $\mathbf{d} = -\tilde{\mathbf{D}}\tilde{\mathbf{x}}_{\mathrm{E}}^{m-1}$. $\mathcal{P}_3^{\text{TPC}}$ is convex and it can be solved directly by the exiting softwares such as CVX. By solving problem $\mathcal{P}_3^{\text{TPC}}$, we can obtain the point in the m-th iteration of the SCA method denoted as $\tilde{\mathbf{x}}_{\mathrm{E}}^{m}$. The SCA solver iterates until it converges and then the transmit ISAC waveform matrix $\mathbf{X}$ can be re-constructed according to (5) and (22).

D. Dual Problem of $\mathcal{P}_3^{TPC}$

Although the CVX tool can be used to directly solve the formulated problem $\mathcal{P}_3^{\text{TPC}}$, the computational efficiency of the scheme can be further improved considering the iterative property. In the remainder of this section we derive the dual problem of $\mathcal{P}_3^{\text{TPC}}$, which can be solved more efficiently.

The Lagrangian dual function of $\mathcal{P}_3^{\text{TPC}}$ is given by

$$\begin{aligned}&\mathcal{L}\left(\tilde{\mathbf{x}}_{\mathrm{E}}, \boldsymbol{\mu}, \nu\right)\\ &= \mathbf{d}^{\mathrm{T}}\tilde{\mathbf{x}}_{\mathrm{E}} + \boldsymbol{\mu}^{\mathrm{T}}\left(t\cdot\mathbf{1} - \tilde{\mathbf{M}}\tilde{\mathbf{x}}_{\mathrm{E}}\right) + \nu\left(\|\tilde{\mathbf{x}}_{\mathrm{E}}\|_2^2 - Lp_0\right),\end{aligned} \tag{28}$$

where $\boldsymbol{\mu} \in \mathbb{R}^{2LK_{\mathrm{u}}\times 1}$ and ν are non-negative dual variables corresponding to inequality constraints (27a) and (27b), respectively. The corresponding KKT conditions can be formulated as

$$\frac{\partial\mathcal{L}}{\partial\tilde{\mathbf{x}}_{\mathrm{E}}} = \mathbf{d} - \tilde{\mathbf{M}}^{\mathrm{T}}\boldsymbol{\mu} + 2\nu\tilde{\mathbf{x}}_{\mathrm{E}} = 0, \tag{29a}$$

$$\boldsymbol{\mu}^{\mathrm{T}}\left(t\cdot\mathbf{1} - \tilde{\mathbf{M}}\tilde{\mathbf{x}}_{\mathrm{E}}\right) = 0, \ \mu_k \geq 0, \ \forall k \leq 2LK_{\mathrm{u}}, \tag{29b}$$

$$\nu\left(\|\tilde{\mathbf{x}}_{\mathrm{E}}\|_2^2 - p_0\right) = 0. \ \nu \geq 0. \tag{29c}$$

According to the KKT conditions, we can deduce that $\nu > 0$. If $\nu = 0$, then no vector $\boldsymbol{\mu}$ can satisfy (29a), which has been proved in Appendix A. This indicates that the total power constraint is active at the point of optimality, i.e.,

$$\|\tilde{\mathbf{x}}_{\mathrm{E}}\|_2^2 = Lp_0. \tag{30}$$

By transforming (29a), we can obtain the expression for the optimal $\tilde{\mathbf{x}}_{\mathrm{E}}$ with respect to Lagrange multipliers:

$$\tilde{\mathbf{x}}_{\mathrm{E}} = \frac{1}{2\nu}\left(\tilde{\mathbf{M}}^{\mathrm{T}}\boldsymbol{\mu} - \mathbf{d}\right). \tag{31}$$

Note that $\mathcal{P}_3^{\mathrm{TPC}}$ is convex and satisfies the Slater's condition [38]. Therefore, the optimal solution of $\mathcal{P}_3^{\mathrm{TPC}}$ can be obtained by solving its dual problem, with the corresponding objective function as follows:

$$\max_{\boldsymbol{\mu},\nu} \min_{\tilde{\mathbf{x}}_{\mathrm{E}}} \mathcal{L}\left(\tilde{\mathbf{x}}_{\mathrm{E}}, \boldsymbol{\mu}, \nu\right). \tag{32}$$

By incorporating the active total power constraint (30) alongside the optimal structure of $\tilde{\mathbf{x}}_{\mathrm{E}}$ in (31) into (32), we can simplify the objective of the dual problem as

$$\begin{aligned}
&\max_{\boldsymbol{\mu},\nu} \min_{\tilde{\mathbf{x}}_{\mathrm{E}}} \mathcal{L}\left(\tilde{\mathbf{x}}_{\mathrm{E}}, \boldsymbol{\mu}, \nu\right) \\
=&\max_{\boldsymbol{\mu},\nu} \min_{\tilde{\mathbf{x}}_{\mathrm{E}}} \mathbf{d}^{\mathrm{T}}\tilde{\mathbf{x}}_{\mathrm{E}} + \boldsymbol{\mu}^{\mathrm{T}}\left(t\cdot\mathbf{1} - \tilde{\mathbf{M}}\tilde{\mathbf{x}}_{\mathrm{E}}\right) + \nu\left(\|\tilde{\mathbf{x}}_{\mathrm{E}}\|_2^2 - Lp_0\right) \\
=&\min_{\boldsymbol{\mu},\nu} \frac{1}{2\nu}\left\|\tilde{\mathbf{M}}^{\mathrm{T}}\boldsymbol{\mu} - \mathbf{d}\right\|_2^2 - t\cdot\mathbf{1}^{\mathrm{T}}\boldsymbol{\mu}.
\end{aligned} \tag{33}$$

Furthermore, by substituting (31) into (30), the total power constraint is equivalent to

$$\frac{1}{4\nu^2}\left\|\tilde{\mathbf{M}}^{\mathrm{T}}\boldsymbol{\mu} - \mathbf{d}\right\|_2^2 = Lp_0, \tag{34}$$

from which we can obtain the following expression for ν only with respect to $\boldsymbol{\mu}$:

$$\nu = \frac{\left\|\tilde{\mathbf{M}}^{\mathrm{T}}\boldsymbol{\mu} - \mathbf{d}\right\|_2}{2\sqrt{Lp_0}}. \tag{35}$$

Hence, we can refine the objective of the dual problem into an optimization only concerning $\boldsymbol{\mu}$ by substituting the aforementioned expression for ν into (33), which is given as

$$\begin{aligned}
&\min_{\boldsymbol{\mu},\nu} \frac{1}{2\nu}\left\|\tilde{\mathbf{M}}^{\mathrm{T}}\boldsymbol{\mu} - \mathbf{d}\right\|_2^2 - t\cdot\mathbf{1}^{\mathrm{T}}\boldsymbol{\mu} \\
=&\min_{\boldsymbol{\mu}} \sqrt{Lp_0}\left\|\tilde{\mathbf{M}}^{\mathrm{T}}\boldsymbol{\mu} - \mathbf{d}\right\|_2 - t\cdot\mathbf{1}^{\mathrm{T}}\boldsymbol{\mu}.
\end{aligned} \tag{36}$$

Considering that all the elements in $\boldsymbol{\mu}$ are non-negative, the dual problem of $\mathcal{P}_3^{\mathrm{TPC}}$ can finally be formulated as follows

$$\mathcal{P}_4^{\mathrm{TPC}}: \min_{\boldsymbol{\mu}} \quad \mathcal{F}\left(\boldsymbol{\mu}\right) = \sqrt{Lp_0}\left\|\tilde{\mathbf{M}}^{\mathrm{T}}\boldsymbol{\mu} - \mathbf{d}\right\|_2 - t\cdot\mathbf{1}^{\mathrm{T}}\boldsymbol{\mu} \tag{37}$$

$$\text{s.t.} \quad \mu_k \geq 0, \ \forall k \in \{1, \cdots, 2LK_{\mathrm{u}}\}. \tag{37a}$$

Note that the problem $\mathcal{P}_4^{\mathrm{TPC}}$ can be more efficiently solved than the problem $\mathcal{P}_3^{\mathrm{TPC}}$ via the Hooke-Jeeves pattern search algorithm [39]. The Hooke-Jeeves pattern search algorithm is an iterative derivative-free method. At each iteration, we first probe the vector $\boldsymbol{\mu}$ along each dimension with a fixed step size to detect the most favorable descent direction. If no further improvement can be achieved, the step size is halved. It can be observed that the problem $\mathcal{P}_4^{\mathrm{TPC}}$ has extremely simple constraints, which allows it to be solved by the Hooke-Jeeves pattern search algorithm with markedly reduced computational complexity. After solving the dual problem $\mathcal{P}_4^{\mathrm{TPC}}$, we can obtain $\boldsymbol{\mu}^*$ and then we can obtain $\tilde{\mathbf{x}}_{\mathrm{E}}^*$ of $\mathcal{P}_3^{\mathrm{TPC}}$ via (31).

In conclusion, the uniform CI-based precoding design for both symbol level and block level under the total power constraint can be summarized in Algorithm 1. Here, we define $N_{\max_1}$ as the upper limit of iterations and ϵ_{th_1} as the convergence condition threshold.

Algorithm 1 CI-based Precoding Design under Total Power Constraint

1: **Input**: $\mathbf{S} = [\mathbf{s}[1], \cdots, \mathbf{s}[L]]$, $\mathbf{H} = [\mathbf{h}_1, \cdots, \mathbf{h}_{K_{\mathrm{u}}}]^{\mathrm{T}}$, $\mathbf{a}(\theta_1), \cdots, \mathbf{a}(\theta_{K_{\mathrm{t}}})$, σ_{max}, Γ, p_0, ϵ_{th_1}, N_{max_1}
2: **Initialization**: $\tilde{\mathbf{x}}_{\mathrm{E}}^0 \in \mathcal{Q}_{\mathrm{TPC}}$, $\tilde{\mathbf{M}}$, $\tilde{\mathbf{D}}$, t, $m = 1$
3: **repeat**
4: Calculate the gradient $\bigtriangledown f\left(\tilde{\mathbf{x}}_{\mathrm{E}}^{m-1}\right)$ by (26);
5: Obtain $\boldsymbol{\mu}^*$ by Hooke-Jeeves pattern search algorithm;
6: Calculate $\tilde{\mathbf{x}}_{\mathrm{E}}^m$ by (31);
7: $m = m + 1$;
8: **until** $\left|f\left(\tilde{\mathbf{x}}_{\mathrm{E}}^{m-1}\right) - f\left(\tilde{\mathbf{x}}_{\mathrm{E}}^{m-2}\right)\right| < \epsilon_{\mathrm{th}_1}$ or $m > N_{max_1}$.
9: Calculate $\mathbf{X}$ from $\tilde{\mathbf{x}}_{\mathrm{E}}^m$ according to (5) and (22).
10: **Output**: $\mathbf{X} = [\mathbf{x}[1], \cdots, \mathbf{x}[L]]$

E. Analysis on Complexity and Convergence

Under the total power constraint, the computational complexity of the CI-based precoding design mainly comes from solving the optimization problem $\mathcal{P}_3^{\mathrm{TPC}}$.

Firstly, we analyze the computational complexity of problem $\mathcal{P}_3^{\mathrm{TPC}}$ with CVX. Since problem $\mathcal{P}_3^{\mathrm{TPC}}$ is a convex optimization problem and involves only linear matrix inequality (LMI) and second-order cone (SOC) constraints, it can be solved by a standard interior-point method (IPM) embedded in CVX. Generally, the computational complexity of the IPM consists of two parts: (1) iteration complexity and (2) per-iteration computation cost [40]. The total number of decision variables in the optimization problem $\mathcal{P}_3^{\mathrm{TPC}}$ is $n = 2LN$, and problem $\mathcal{P}_3^{\mathrm{TPC}}$ includes $2LK_{\mathrm{u}}$ LMI constraints of size 1 as well as one SOC constraint of size $2LN$. Given an accuracy threshold ϵ, the number of iterations required to reach an ϵ-optimal solution is on the order of $\sqrt{\varphi(\mathcal{K})}\cdot\ln(1/\epsilon)$, where $\varphi(\mathcal{K}) = 2LK_{\mathrm{u}} + 2$ is the so-called barrier parameter. In each iteration, the required computational complexity is on the order of $\left[n(2LK_{\mathrm{u}}) + n^2(2LK_{\mathrm{u}}) + n(2LN)^2 + n^3\right]$, which can be written as $\mathcal{O}\left(L^3N^3\right)$. Therefore, the computational complexity of solving problem $\mathcal{P}_3^{\mathrm{TPC}}$ with CVX can be expressed as $\ln(1/\epsilon)\cdot\sqrt{2LK_{\mathrm{u}}+2}\cdot\mathcal{O}\left(L^3N^3\right)$.

Next, we analyze the computational complexity of solving the dual problem $\mathcal{P}_4^{\mathrm{TPC}}$ by the Hooke-Jeeves pattern search method. In Hooke-Jeeves pattern search method, the maximum number of iterations is set as $I_{\max_1}$. In each iteration, we need to calculate the objective function $\mathcal{F}(\boldsymbol{\mu})$ $4LK_{\mathrm{u}}$ times, and each time with computational complexity order of $(2LK_{\mathrm{u}})(2LN)$. Therefore, the computational complexity of solving problem $\mathcal{P}_4^{\mathrm{TPC}}$ by the Hooke-Jeeves pattern search algorithm is $I_{\max_1}\cdot\mathcal{O}\left(L^3NK_{\mathrm{u}}^2\right)$, which is much lower than that solved by problem $\mathcal{P}_3^{\mathrm{TPC}}$ with CVX.

Although iterative method is employed in Algorithm 1, it is easy to verify that the convergence of the proposed iterative algorithm is always guaranteed. With the help of the SCA method, we can always find a solution that is not worse than the one from the previous iteration. Therefore, the

objective function value of the optimization problem $\mathcal{P}_2^{\text{TPC}}$ is monotonically non-decreasing with the increase in the number of iterations. Moreover, the convergence of the proposed algorithm will be further demonstrated through simulation results in Section V.

IV. Precoding Design under Per-antenna Power Constraint

In practical systems, each transmit antenna is usually equipped with its dedicated power amplifier. Therefore, it is more realistic to design ISAC precoding approaches that incorporate the per-antenna power constraint [41]–[43]. In this section we design the transmit ISAC waveform matrix $\mathbf{X}$ under per-antenna power constraint.

A. Problem Formulation

The CI-SLP and the CI-BLP optimization problem for ISAC system under per-antenna power constraint can be uniformly formulated as

$$\mathcal{P}_1^{\text{PAPC}}: \min_{\{\mathbf{x}_{\text{E},l}\}} -\sum_{l=1}^{L}\mathbf{x}_{\text{E},l}^{\text{T}}\mathbf{D}\mathbf{x}_{\text{E},l} \tag{38}$$

$$\text{s.t.} \quad \mathbf{M}_l\mathbf{x}_{\text{E},l} \geq t, \forall l \in \{1,\cdots,L\}, \tag{38a}$$

$$\sum_{l=1}^{L}\left(|x_{n,l}|^2+|x_{n+N,l}|^2\right) \leq \frac{Lp_0}{N},\ \forall n \in \mathcal{N}, \tag{38b}$$

where $x_{n,l}$ represents the n-th element in $\mathbf{x}_{\text{E},l}$ and $\mathcal{N} = \{1,2,\cdots,N\}$. The per-antenna power constraint (38b) in $\mathcal{P}_1^{\text{PAPC}}$ is a convex constraint. Similarly, $\mathcal{P}_1^{\text{PAPC}}$ can be expressed more concisely as

$$\mathcal{P}_2^{\text{PAPC}}: \min_{\tilde{\mathbf{x}}_{\text{E}}} -\tilde{\mathbf{x}}_{\text{E}}^{\text{T}}\tilde{\mathbf{D}}\tilde{\mathbf{x}}_{\text{E}} \tag{39}$$

$$\text{s.t.} \quad \tilde{\mathbf{M}}\tilde{\mathbf{x}}_{\text{E}} \geq t, \tag{39a}$$

$$\tilde{\mathbf{x}}_{\text{E}}^{\text{T}}\tilde{\mathbf{E}}_n\tilde{\mathbf{x}}_{\text{E}} \leq \frac{Lp_0}{N},\ \forall n \in \mathcal{N}, \tag{39b}$$

where $\tilde{\mathbf{x}}_{\text{E}}$, $\tilde{\mathbf{D}}$ and $\tilde{\mathbf{M}}$ have been defined in (22) and (23). In addition, $\tilde{\mathbf{E}}_n$ is defined as

$$\tilde{\mathbf{E}}_n = \mathbf{I}_L \otimes \mathbf{E}_n, \tag{40}$$

where

$$\mathbf{E}_n = \mathbf{\Delta}_1^{\text{T}}\mathbf{e}_n\mathbf{e}_n^{\text{T}}\mathbf{\Delta}_1 + \mathbf{\Delta}_2^{\text{T}}\mathbf{e}_n\mathbf{e}_n^{\text{T}}\mathbf{\Delta}_2,$$
$$\mathbf{\Delta}_1 = \begin{bmatrix}\mathbf{I}_N & \mathbf{0}\\ \mathbf{0} & \mathbf{I}_N\end{bmatrix}, \mathbf{\Delta}_2 = \begin{bmatrix}\mathbf{0} & \mathbf{I}_N\\ \mathbf{I}_N & \mathbf{0}\end{bmatrix}, \tag{41}$$

and $\mathbf{e}_n \in \mathbb{R}^{2N}$ is a vector where its n-th entry is 1 and the other elements are 0.

B. Algorithm Design with SCA Transformation

Problem $\mathcal{P}_2^{\text{PAPC}}$ is also a non-convex problem because of the non-convex objective function. In this section, we solve the non-convex problem $\mathcal{P}_2^{\text{PAPC}}$ by leveraging the SCA procedure similar to Section III-C.

First, we define $\mathcal{Q}_{\text{PAPC}}$ as the feasible region of $\mathcal{P}_2^{\text{PAPC}}$ constrained by (39a) and (39b), which is a convex set of $\tilde{\mathbf{x}}_{\text{E}}$. The optimization problem we need to solve in the m-th iteration of the SCA solver can be expressed as

$$\mathcal{P}_3^{\text{PAPC}}: \min_{\tilde{\mathbf{x}}_{\text{E}}} \mathbf{d}^{\text{T}}\tilde{\mathbf{x}}_{\text{E}} \tag{42}$$

$$\text{s.t.} \quad \tilde{\mathbf{M}}\tilde{\mathbf{x}}_{\text{E}} \geq t, \tag{42a}$$

$$\tilde{\mathbf{x}}_{\text{E}} \in \mathcal{X}, \tag{42b}$$

where $\mathcal{X} \subseteq \mathbb{R}^{2LN}$ is a convex set and it is defined as

$$\mathcal{X} = \left\{\tilde{\mathbf{x}}_{\text{E}} | \tilde{\mathbf{x}}_{\text{E}}^{\text{T}}\tilde{\mathbf{E}}_n\tilde{\mathbf{x}}_{\text{E}} \leq \frac{Lp_0}{N},\ \forall n \in \mathcal{N}\right\}. \tag{43}$$

Since $\mathcal{P}_3^{\text{PAPC}}$ is a convex optimization problem, it can be solved directly by CVX. Through solving problem $\mathcal{P}_3^{\text{PAPC}}$, we can obtain $\tilde{\mathbf{x}}_{\text{E}}^m$. After the convergence of the SCA solver, the transmit ISAC waveform matrix $\mathbf{X}$ can be obtained according to (5) and (22).

C. Simple Parallel Algorithm for $\mathcal{P}_3^{PAPC}$

The efficient algorithm for solving the dual problem of $\mathcal{P}_3^{\text{TPC}}$ in Section III-D is designed for the total power constraint which cannot be directly applied to $\mathcal{P}_3^{\text{PAPC}}$ for system with per-antenna power constraint, and the specific reasons have been analyzed in Appendix B.

Hence, we adopt a simple parallel algorithm in [32] to solve the optimization problem $\mathcal{P}_3^{\text{PAPC}}$. This simple parallel algorithm is similar to the classical dual subgradient algorithm with primal averaging, which deals with the objective and constraints parallelly. However, this simple parallel algorithm can perform a faster convergence rate than the dual subgradient algorithm, which has been proved in [32].

In order to solve problem $\mathcal{P}_3^{\text{PAPC}}$ in a parallel way, we first define the inequality constraint function (42a) in $\mathcal{P}_3^{\text{PAPC}}$ as

$$\mathbf{g}\left(\tilde{\mathbf{x}}_{\text{E}}\right) = t\cdot\mathbf{1} - \tilde{\mathbf{M}}\tilde{\mathbf{x}}_{\text{E}}. \tag{44}$$

In addition, we define the primal variables as vectors $\hat{\mathbf{x}}(i)$ and the virtual queues as vectors $\mathbf{Q}(i)$. $\mathbf{Q}(i)$ are called as virtual queues because they update like queueing equations and can be viewed as dual variables because they have a close connection to Lagrange multipliers.

In the i-th iteration of the simple parallel algorithm, the vector $\hat{\mathbf{x}}(i) \in \mathcal{X}$ can be updated as

$$\hat{\mathbf{x}}(i) = \underset{\hat{\mathbf{x}}\in\mathcal{X}}{\text{argmin}}\ \mathbf{d}^{\text{T}}\hat{\mathbf{x}} + \left[\mathbf{Q}(i) + \mathbf{g}\left(\hat{\mathbf{x}}(i-1)\right)\right]^{\text{T}}\mathbf{g}\left(\hat{\mathbf{x}}\right) + \alpha\left\|\hat{\mathbf{x}} - \hat{\mathbf{x}}(i-1)\right\|^2. \tag{45}$$

It is easy to note that the structure of the objective function in (45) is different from that of the general Lagrange function. Here, $\mathbf{g}\left(\hat{\mathbf{x}}(i-1)\right)$ obtained in the previous iteration is added to $\mathbf{Q}(i)$, and $\mathbf{g}\left(\hat{\mathbf{x}}(i-1)\right)$ is multiplied by the constraint function $\mathbf{g}\left(\hat{\mathbf{x}}\right)$, producing a new cross-product term. This cross-product term together with another newly introduced quadratic term $\alpha\left\|\hat{\mathbf{x}} - \hat{\mathbf{x}}(i-1)\right\|^2$ can leads to a faster convergence rate. Note that $\hat{\mathbf{x}}(i-1)$ is the primal variable obtained in the previous iteration, and $\alpha > 0$ is the coefficient of the newly introduced quadratic term. Then, we update $\mathbf{Q}(i+1)$ via

$$\mathbf{Q}(i+1) = \max\left\{-\mathbf{g}\left(\hat{\mathbf{x}}(i)\right), \mathbf{Q}(i) + \mathbf{g}\left(\hat{\mathbf{x}}(i)\right)\right\}. \tag{46}$$

Here is an important difference from the classical dual subgradient algorithm. The traditional update rule is $\mathbf{Q}(i+1) = \max\{\mathbf{0}, \mathbf{Q}(i) + \mathbf{g}(\hat{\mathbf{x}}(i))\}$ [44], while in the simple parallel algorithm, the update equation for $\mathbf{Q}$ is modified to take a max with $-\mathbf{g}(\hat{\mathbf{x}}(i))$, rather than simply project onto the non-negative real numbers.

Next, the average result over the first $(i+1)$ iterations can be expressed as

$$\bar{\mathbf{x}}(i+1) = \frac{1}{i+1}\sum_{\tau=0}^{i}\hat{\mathbf{x}}(\tau) = \bar{\mathbf{x}}(i)\frac{i}{i+1} + \hat{\mathbf{x}}(i)\frac{1}{i+1}. \quad (47)$$

We average the results of all the primal variables from the iterations, and the vector $\bar{\mathbf{x}}(i)$ obtained at convergence can closely approximate the optimal solution to $\mathcal{P}_3^{\text{PAPC}}$ [32].

In the simple parallel algorithm, we use an initial vector represented as $\hat{\mathbf{x}}(-1)$ which is chosen as any vector in $\mathcal{X}$ that satisfying the per-antenna power constraint. In addition, we further define a vector $\mathbf{Q}(0) = \max\{\mathbf{0}, -\mathbf{g}(\hat{\mathbf{x}}(-1))\}$ as initialization. The designed simple parallel algorithm for solving $\mathcal{P}_3^{\text{PAPC}}$ can be summarized in Algorithm 2, where $I_{\max_2}$ is the upper limit of iterations and ϵ_{th_2} represents the convergence condition threshold.

Algorithm 2 Simple Parallel Algorithm

1: **Input**: $\tilde{\mathbf{M}}$, $\mathbf{d}$, L, N, p_0, $I_{\max_2}$, ϵ_{th_2}
2: **Initialization**: $\hat{\mathbf{x}}(-1) \in \mathcal{X}$, $\bar{\mathbf{x}}(-1) \in \mathcal{X}$, $\mathbf{Q}(0) = \max\{\mathbf{0}, -\mathbf{g}(\hat{\mathbf{x}}(-1))\}$, $i = 0$
3: **while** $i \le I_{\max_2}$ **do**
4: Update $\hat{\mathbf{x}}(i)$ by solving problem (45);
5: Update $\mathbf{Q}(i+1)$ by (46);
6: Update $\bar{\mathbf{x}}(i+1)$ by (47);
7: $i = i+1$;
8: **if** $\|\bar{\mathbf{x}}(i) - \bar{\mathbf{x}}(i-1)\|_2^2 \le \epsilon_{\text{th}_2}$ **then**
9: Go to 12;
10: **end if**
11: **end while**
12: $\tilde{\mathbf{x}}_{\text{E}}^* = \bar{\mathbf{x}}(i)$.
13: **Output**: $\tilde{\mathbf{x}}_{\text{E}}^*$

D. ADMM Algorithm for Updating $\hat{\mathbf{x}}(i)$

One essential step in Algorithm 2 is for solving the problem (45) to update the vector $\hat{\mathbf{x}}(i)$. Here, we try to leverage the ADMM algorithm to develop an efficient solution for updating $\hat{\mathbf{x}}(i)$. In the ADMM framework, first of all, it is necessary to introduce a new variable $\mathbf{z}$ and an indicator function as

$$I_{\mathcal{X}}(\mathbf{z}) = \begin{cases} 0, & \text{if } \mathbf{z} \in \mathcal{X}, \\ \infty, & \text{otherwise.} \end{cases} \quad (48)$$

Then we further define the objective function in (45) as:

$$\begin{aligned} h(\hat{\mathbf{x}}) &= \mathbf{d}^{\mathrm{T}}\hat{\mathbf{x}} + [\mathbf{Q}(i) + \mathbf{g}(\hat{\mathbf{x}}(i-1))]^{\mathrm{T}}\mathbf{g}(\hat{\mathbf{x}}) \\ &\quad + \alpha\|\hat{\mathbf{x}} - \hat{\mathbf{x}}(i-1)\|^2 \\ &= \mathbf{d}^{\mathrm{T}}\hat{\mathbf{x}} + \hat{\mathbf{q}}^{\mathrm{T}}\left(t\cdot\mathbf{1} - \tilde{\mathbf{M}}\hat{\mathbf{x}}\right) + \alpha\|\hat{\mathbf{x}} - \hat{\mathbf{x}}(i-1)\|^2, \end{aligned} \quad (49)$$

where $\hat{\mathbf{q}} = \mathbf{Q}(i) + \mathbf{g}(\hat{\mathbf{x}}(i-1))$. Hence, the optimization problem in (45) can be equivalently written as a consensus form:

$$\begin{aligned} \mathcal{P}_4^{\text{PAPC}}: \ &\min_{\hat{\mathbf{x}},\mathbf{z}} \ h(\hat{\mathbf{x}}) + I_{\mathcal{X}}(\mathbf{z}) \\ &\text{s.t. } \hat{\mathbf{x}} - \mathbf{z} = \mathbf{0}, \end{aligned} \quad (50)$$

where $I_{\mathcal{X}}(\mathbf{z})$ is utilized as a penality and it approaches infinity if $\mathbf{z}$ does not in $\mathcal{X}$. The augmented Lagrange function for the optimization problem $\mathcal{P}_4^{\text{PAPC}}$can be expressed as

$$\begin{aligned} &L_\rho(\hat{\mathbf{x}}, \mathbf{z}, \mathbf{y}) \\ &= h(\hat{\mathbf{x}}) + I_{\mathcal{X}}(\mathbf{z}) + \mathbf{y}^{\mathrm{T}}(\hat{\mathbf{x}} - \mathbf{z}) + \frac{\rho}{2}\|\hat{\mathbf{x}} - \mathbf{z}\|_2^2 \\ &= \mathbf{d}^{\mathrm{T}}\hat{\mathbf{x}} + \hat{\mathbf{q}}^{\mathrm{T}}\left(t\cdot\mathbf{1} - \tilde{\mathbf{M}}\tilde{\mathbf{x}}_{\text{E}}\right) + \alpha\|\hat{\mathbf{x}} - \hat{\mathbf{x}}(i-1)\|^2 \\ &\quad + I_{\mathcal{X}}(\mathbf{z}) + \mathbf{y}^{\mathrm{T}}(\hat{\mathbf{x}} - \mathbf{z}) + \frac{\rho}{2}\|\hat{\mathbf{x}} - \mathbf{z}\|_2^2. \end{aligned} \quad (51)$$

Here, the elements in $\mathbf{y} \in \mathbb{R}^{2LN\times 1}$ are dual variables, and $\rho > 0$ is the penalty parameter for guaranteeing the equality constraint in $\mathcal{P}_4^{\text{PAPC}}$. The update process for $\hat{\mathbf{x}}$, $\mathbf{z}$, and $\mathbf{y}$is as follows

$$\hat{\mathbf{x}}^{loop+1} = \underset{\hat{\mathbf{x}}}{\text{argmin}} \ L_\rho\left(\hat{\mathbf{x}}, \mathbf{z}^{loop}, \mathbf{y}^{loop}\right), \quad (52)$$

$$\mathbf{z}^{loop+1} = \underset{\mathbf{z}}{\text{argmin}} \ L_\rho\left(\hat{\mathbf{x}}^{loop+1}, \mathbf{z}, \mathbf{y}^{loop}\right), \quad (53)$$

$$\mathbf{y}^{loop+1} = \mathbf{y}^{loop} + \rho\left(\hat{\mathbf{x}}^{loop+1} - \mathbf{z}^{loop+1}\right). \quad (54)$$

Specifically, the subproblem for updating $\hat{\mathbf{x}}$ can be written as

$$\begin{aligned} \min_{\hat{\mathbf{x}}} \ &\mathbf{d}^{\mathrm{T}}\hat{\mathbf{x}} - \hat{\mathbf{q}}^{\mathrm{T}}\tilde{\mathbf{M}}\hat{\mathbf{x}} + \alpha\|\hat{\mathbf{x}} - \hat{\mathbf{x}}(i-1)\|^2 + \mathbf{y}^{\mathrm{T}}\hat{\mathbf{x}} \\ &+ \frac{\rho}{2}\|\hat{\mathbf{x}} - \mathbf{z}\|_2^2. \end{aligned} \quad (55)$$

where the objective is convex versus $\hat{\mathbf{x}}$. Hence, we can obtain the optimal $\hat{\mathbf{x}}$ by letting the derivative of the objective function in (55) with respect to $\hat{\mathbf{x}}$ be zero as given below

$$\begin{aligned} &\mathbf{d} - \tilde{\mathbf{M}}^{\mathrm{T}}\hat{\mathbf{q}} + 2\alpha(\hat{\mathbf{x}} - \hat{\mathbf{x}}(i-1)) + \mathbf{y} + \rho(\hat{\mathbf{x}} - \mathbf{z}) = \mathbf{0} \\ \Rightarrow &\hat{\mathbf{x}} = \frac{1}{2\alpha+\rho}\left(\tilde{\mathbf{M}}^{\mathrm{T}}\hat{\mathbf{q}} - \mathbf{d} + 2\alpha\hat{\mathbf{x}}(i-1) - \mathbf{y} + \rho\mathbf{z}\right). \end{aligned} \quad (56)$$

In addition, the subproblem for updating $\mathbf{z}$ can be written as

$$\min_{\mathbf{z}} \ I_{\mathcal{X}}(\mathbf{z}) - \mathbf{y}^{\mathrm{T}}\mathbf{z} + \frac{\rho}{2}\|\hat{\mathbf{x}} - \mathbf{z}\|_2^2. \quad (57)$$

By letting the derivative of the objective function in (57) with respect to $\mathbf{z}$ be zero, the optimal $\mathbf{z}$ can be obtained:

$$\begin{aligned} &\partial I_{\mathcal{X}}(\mathbf{z}) - \mathbf{y} - \rho(\hat{\mathbf{x}} - \mathbf{z}) = \mathbf{0} \\ \Rightarrow &\mathbf{z} = \Pi_{\mathcal{X}}\left(\hat{\mathbf{x}} + \frac{\mathbf{y}}{\rho}\right). \end{aligned} \quad (58)$$

where $\Pi_{\mathcal{X}}(\cdot)$ is a projection operator, and $\Pi_{\mathcal{X}}(\hat{\mathbf{z}})$ denotes the projection of the vector $\hat{\mathbf{z}}$ onto the set $\mathcal{X}$. For any $\hat{\mathbf{z}} \in \mathbb{R}^{2LN\times 1}$, $\Pi_{\mathcal{X}}(\hat{\mathbf{z}})$ can be implemented in a closed form as (59) on the top of the next page.

According to the above analysis, the corresponding ADMM algorithm is summarized in Algorithm 3. Here, $I_{\max_3}$ and ϵ_{th_3} represent the upper limit of iterations and the convergence condition threshold, respectively.

$$\left(\Pi_{\mathcal{X}}\left(\hat{z}_n\right),\Pi_{\mathcal{X}}\left(\hat{z}_{n+N}\right),\cdots,\Pi_{\mathcal{X}}\left(\hat{z}_{n+(2L-1)N}\right)\right) = \begin{cases} \left(\hat{z}_n,\hat{z}_{n+N},\cdots,\hat{z}_{n+(2L-1)N}\right), & \text{if } \sum_{\hat{l}=0}^{2L-1}\hat{z}^2_{n+(2\hat{l}-1)N} \le \frac{Lp_0}{N}, \\ \frac{\sqrt{Lp_0}}{\sqrt{N\sum_{\hat{l}=0}^{2L-1}\hat{z}^2_{n+(2\hat{l}-1)N}}}\left(\hat{z}_n,\hat{z}_{n+N},\cdots,\hat{z}_{n+(2L-1)N}\right), & \text{otherwise.} \end{cases} \tag{59}$$

Algorithm 3 ADMM Algorithm

Input: $\mathbf{d}$, $\hat{\mathbf{q}}$, $\tilde{\mathbf{M}}$, α, ρ, L, N, p_0, $I_{\max_3}$, ϵ_{th_3}
Initialization: $\mathbf{z}^1 \in \mathcal{X}$, $\mathbf{y}^1 = \mathbf{0}$, $loop = 1$
while $loop \le I_{\max_3}$ **do**
  Compute $\hat{\mathbf{x}}^{loop+1}$ by (56);
  Compute $\mathbf{z}^{loop+1}$ by (58);
  Update $\mathbf{y}^{loop+1}$ by (54);
  $loop = loop + 1$;
  if $\left\|\mathbf{z}^{loop+1} - \mathbf{z}^{loop}\right\|_2^2 \le \epsilon_{\text{th}_3}$ **then**
    Go to 12;
  end if
end while
$\hat{\mathbf{x}}(i) = \mathbf{z}^{loop}$.
Output: $\hat{\mathbf{x}}(i)$

In conclusion, the uniform CI-based precoding design for both symbol and block levels under per-antenna power constraint can be summarized in Algorithm 4 with $N_{\max_4}$ and ϵ_{th_4} being the maximum iteration and the convergence threshold.

Algorithm 4 CI-based Precoding Design under Per-Antenna Power Constraint

Input: $\mathbf{S} = [\mathbf{s}[1],\cdots,\mathbf{s}[L]]$, $\mathbf{H} = [\mathbf{h}_1,\cdots,\mathbf{h}_{K_{\text{u}}}]^{\text{T}}$, $\mathbf{a}(\theta_1),\cdots,\mathbf{a}(\theta_{K_{\text{t}}})$, σ_{max}, Γ, p_0, $N_{\max_4}$, ϵ_{th_4}
Initialization: Initial $\tilde{\mathbf{x}}_{\text{E}}^0 \in \mathcal{Q}_{\text{PAPC}}$, $\tilde{\mathbf{M}}$, $\tilde{\mathbf{D}}$, t, $m = 1$
repeat
  Calculate the gradient $\bigtriangledown f\left(\tilde{\mathbf{x}}_{\text{E}}^{m-1}\right)$ by (26);
  Obtain $\tilde{\mathbf{x}}_{\text{E}}^m$ by Algorithm 2.
  $m = m + 1$.
until $\left|f\left(\tilde{\mathbf{x}}_{\text{E}}^{m-1}\right) - f\left(\tilde{\mathbf{x}}_{\text{E}}^{m-2}\right)\right| < \epsilon_{\text{th}_4}$ or $m > N_{\max_4}$.
Calculate $\mathbf{X}$ from $\tilde{\mathbf{x}}_{\text{E}}^m$ according to (5) and (22).
Output: $\mathbf{X} = [\mathbf{x}[1],\cdots,\mathbf{x}[L]]$

E. Analysis on Complexity and Convergence

Under the per-antenna power constraint, the computational complexity of the CI-based precoding design mainly comes from solving the optimization problem $\mathcal{P}_3^{\text{PAPC}}$.

Firstly, we analyze the computational complexity of problem $\mathcal{P}_3^{\text{PAPC}}$ with CVX. Since problem $\mathcal{P}_3^{\text{PAPC}}$ is also a convex optimization problem and involves only LMI and SOC constraints, it can be solved by the IPM embedded in CVX. The total number of decision variables in the optimization problem $\mathcal{P}_3^{\text{PAPC}}$ is $n = 2LN$, and problem $\mathcal{P}_3^{\text{PAPC}}$ includes $2LK_{\text{u}}$ LMI constraints of size 1 as well as one SOC constraint of size $2LN$. The number of iterations required to reach an ϵ-optimal solution is on the order of $\sqrt{\varphi(\mathcal{K})}\cdot\ln(1/\epsilon)$. In each iteration, the required computational complexity is on the order of $\left[n(2LK_{\text{u}}) + n^2(2LK_{\text{u}}) + nN(2LN)^2 + n^3\right]$, which can be written as $\mathcal{O}\left(L^3N^4\right)$. Therefore, the computational complexity of solving problem $\mathcal{P}_3^{\text{PAPC}}$ with CVX can be expressed as $\ln(1/\epsilon)\cdot\sqrt{2LK_{\text{u}}+2N}\cdot\mathcal{O}\left(L^3N^4\right)$.

Next, we analyze the computational complexity of solving $\mathcal{P}_3^{\text{PAPC}}$ with the designed simple parallel algorithm. In the designed simple parallel algorithm, the maximum number of iterations is set as $I_{\max_2}$. In each iteration, the computational complexity mainly arises from solving the problem (45) via the ADMM algorithm, and the computational complexity required for ADMM is on the order of $I_{\max_3}(2LN)(2LK_{\text{u}})$. Therefore, the computational complexity of solving problem $\mathcal{P}_3^{\text{PAPC}}$ with the designed simple parallel algorithm is $I_{\max_2}I_{\max_3}\mathcal{O}\left(L^2NK_{\text{u}}\right)$, which is much lower than that solved by CVX.

The convergence of the simple parallel algorithm and the ADMM algorithm is proven in [32] and [31], respectively. Similar to Algorithm 1, with the help of the SCA method, we can always find a solution that is not worse than the one from the previous iteration. Therefore, the objective function value of the optimization problem $\mathcal{P}_2^{\text{PAPC}}$ is also monotonically non-decreasing with the increase in the number of iterations. The convergence of the proposed algorithm will be further demonstrated through simulation results in Section V.

V. Simulation Results

In this section, numerical results are provided to validate the aforementioned derivations, and demonstrate the superiority of the proposed algorithms for CI-SLP and CI-BLP schemes in enhancing ISAC performance. This section first presents the convergence behavior of the proposed algorithms, and the remaining content can be divided into two parts: simulation results under total power constraint and simulation results under per-antenna power constraint. The proposed schemes are compared with the the previous scheme in terms of SER performance, transmit beampattern, tradeoff between communication SER and radar DP, and execution time. In this section, standard Rayleigh fading channels are employed for communications, while line-of-sight path is considered for radar illumination. The simulation results of radar beampattern are the average of multiple samples, which is commonly used in practical systems and can well smooth away the undesired instantaneous sidelobes. The simulation results of the execution time are obtained from Matlab 2023 installed in a Windows 11 Desktop with CPU i5-12400.

The abbreviations of the considered precoding schemes in the simulation are as follows:

1) IC-BLP with SDR: SDR in [10], which is a conventional

BLP scheme for ISAC, and it aims at interference cancellation (IC) rather than interference exploitation.
2) Proposed CI-SLP: The proposed CI-SLP scheme for ISAC system.
3) Proposed CI-BLP: The proposed CI-BLP scheme for ISAC system.

Throughout the simulations, the transmit power budget per symbol slot is set as $p_0 = 30$dBm, and QPSK modulation is employed. The length of the considered block for CI-BLP scheme is $L = 6$. We calculate the radar DP based on [45, eq. (69)] and the false-alarm probability for radar is $P_{\mathrm{FA}} = 10^{-7}$. Without specific statements, we set $\sigma_{\max} = 20$dBm and $\Gamma = 4$dB. The given desired beampattern mainlobe width for IC-BLP with SDR scheme is $\Delta_{\mathrm{d}} = 10^{\circ}$.

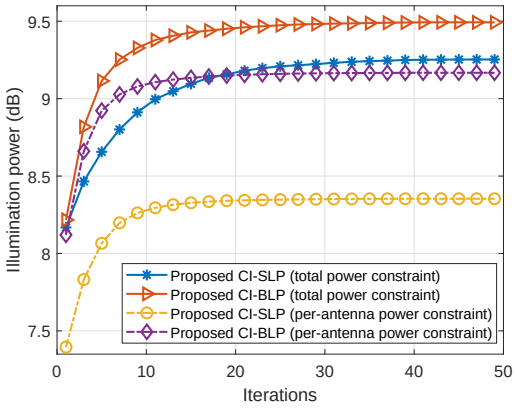

Fig. 2. Illumination power versus the iterations, $N = 10$, $K_{\mathrm{u}} = 3$, $K_{\mathrm{t}} = 1$, $\Gamma = 4$dB, $p_0 = 30$dBm, QPSK.

The convergence behavior of the proposed iterative algorithms are shown in Fig. 2. The simulation results indicate that the illumination power obtained by the algorithms exhibits a monotonically non-decreasing behavior with the increase in iterations. Moreover, the proposed algorithms can rapidly converge to a stable value within tens of iterations. Therefore, the convergence of the proposed algorithms is verified.

A. Simulation Results under Total Power Constraint

Fig. 3 depicts the SER performance of different schemes when $N = 10$ and $K_{\mathrm{u}} = 3$. In Fig. 3, the SER performance of IC-BLP with SDR scheme is significantly worse than that of other schemes, which indicates the communication performance advantages of CI-based schemes. It is observed that the proposed CI-SLP scheme and the proposed CI-BLP scheme show almost the same SER performance, which reflects that the CI constraints can always be satisfied. This also demonstrates the effectiveness of the proposed algorithm in solving the optimization problem under total power constraint.

Fig. 4 depicts the transmit beampatterns of different schemes with multiple targets, and their locations are $\theta_1 = -40^{\circ}$, $\theta_2 = 0^{\circ}$, and $\theta_3 = 40^{\circ}$, respectively. It can be seen that the illumination power of the proposed CI-SLP scheme and the proposed CI-BLP scheme in the target direction is significantly greater than that of IC-BLP with SDR scheme. The sidelobes between the two target directions of the proposed CI-SLP and CI-BLP schemes are also significantly lower than IC-BLP with SDR scheme. This indicates the advantages of the proposed CI-based precoding schemes.

Fig. 5 shows the transmit beampatterns of different schemes with a single target at the location $\theta_1 = 0^{\circ}$. The transmit beampatterns of different schemes for single target detection can be compared more clearly than multi-target detection. The CI-SLP scheme and the CI-BLP scheme proposed in this paper have better transmit beampatterns than IC-BLP with SDR scheme. In addition, the proposed CI-BLP scheme has the best transmit beampattern, due to the fact that CI-BLP scheme has a more relaxed power allocation constraint compared with CI-SLP scheme.

Fig. 6 plots the trade-off between communication SER and radar sensing DP for different schemes as the communication SINR threshold Γ varies from 1dB to 8dB. We set SNR = 15dB for the SER calculation and SNRr = 10dBm for the DP calculation. It can be seen that at the same SER performance, the DP results of the proposed CI-SLP scheme and CI-BLP scheme are better, which more clearly reflects the ISAC performance advantages of the proposed CI-based precoding schemes. This not only benefits from the gain in communication performance achieved by the CI-based precoding, but also benefits from the fact that we directly maximize the illumination power in the target direction, which determines the detection probability directly.

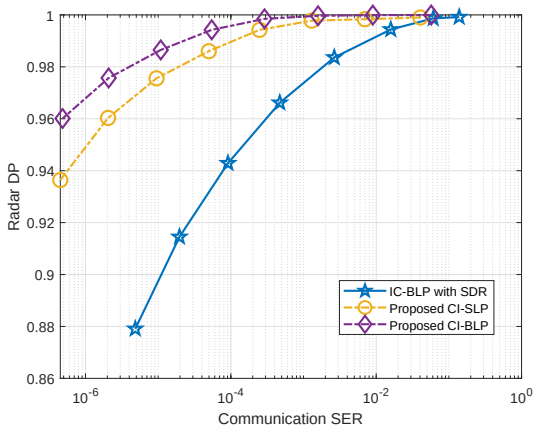

Fig. 6. Tradeoff between the communication SER and radar DP, $N = 10$, $K_{\mathrm{u}} = 3$, $K_{\mathrm{t}} = 1$, SNR = 15dB, SNRr = 10dBm, $p_0 = 30$dBm, QPSK.

Fig. 7 shows the complexity of different schemes in terms of the execution time under total power constraint, with the number of transmit antennas N ranging from 10 to 20. With the increase of the number of transmit antennas, the computational complexity of each scheme will increase correspondingly, because the number of optimization variables in the optimization problem increases. As can be seen, the execution time of the proposed CI-SLP scheme and CI-BLP scheme is even less than that of the IC-BLP with SDR scheme, thanks to the designed low-complexity algorithm. In addition, we can observe that the complexity of CI-SLP scheme is lower than that of CI-BLP scheme because of the smaller size of the optimization problem.

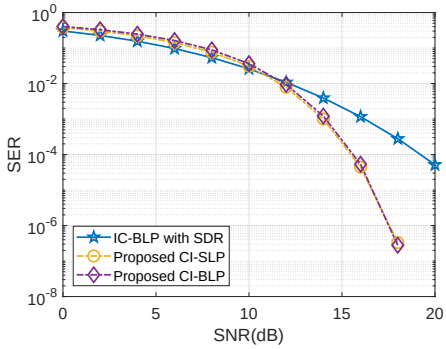

Fig. 3. SER performance, $N = 10$, $K_{\mathrm{u}} = 3$, $\Gamma = 4$dB, $p_0 = 30$dBm, QPSK.

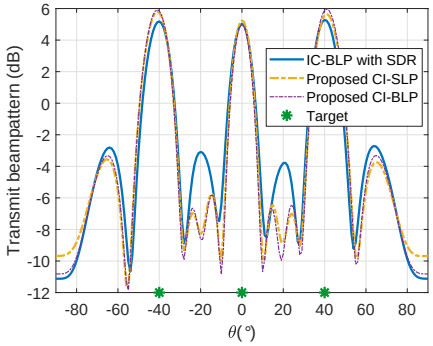

Fig. 4. Transmit beampatterns, $N = 10$, $K_{\mathrm{u}} = 3$, $K_{\mathrm{t}} = 3$, $\Gamma = 4$dB, $p_0 = 30$dBm, QPSK.

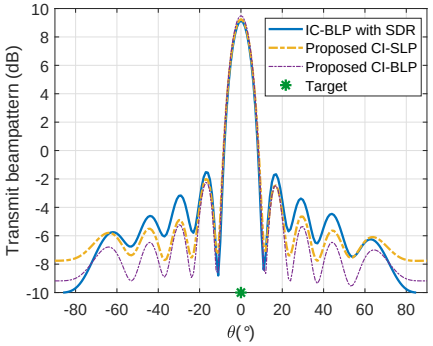

Fig. 5. Transmit beampatterns, $N = 10$, $K_{\mathrm{u}} = 3$, $K_{\mathrm{t}} = 1$, $\Gamma = 4$dB, $p_0 = 30$dBm, QPSK.

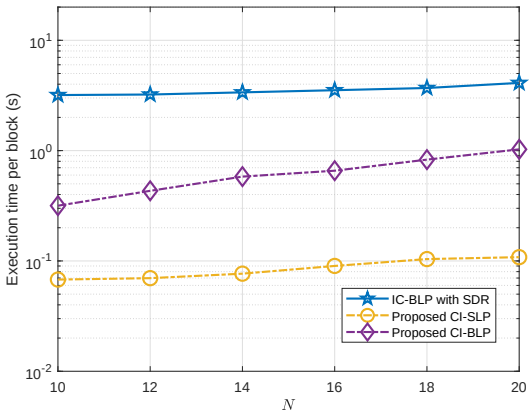

Fig. 7. Execution time of different schemes, $K_{\mathrm{u}} = 3$, $K_{\mathrm{t}} = 1$, $\Gamma = 4$dB, $p_0 = 30$dBm, QPSK.

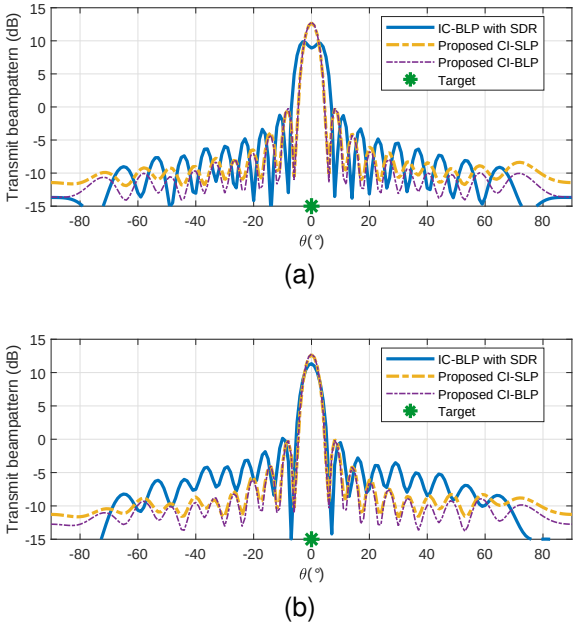

Fig. 8. Transmit beampatterns of different schemes, $N = 20$, $K_{\mathrm{u}} = 3$, $K_{\mathrm{t}} = 1$, $\Gamma = 4$dB, $p_0 = 30$dBm, QPSK. (a) Mainlobe desired beam width $\Delta_{\mathrm{d}} = 10°$. (b) Mainlobe desired beam width $\Delta_{\mathrm{d}} = 6°$.

In addition to the above simulation results, it is interesting to find that when the number of transmit antennas is increased to $N = 20$, the beampattern mainlobe width of the IC-BLP with SDR scheme depends on the given desired beampattern mainlobe width Δ_{d}, since it is optimized to minimize the beampattern MSE. In Fig. 8(a), when $\Delta_{\mathrm{d}} = 10$, the beampattern mainlobe of the IC-BLP with SDR scheme is wider than that of the proposed schemes, and the mainlobe is seriously distorted. In Fig. 8(b), when $\Delta_{\mathrm{d}} = 6$, the mainlobe of the IC-BLP with SDR scheme becomes narrower, but the peak height is still significantly lower than that of the proposed

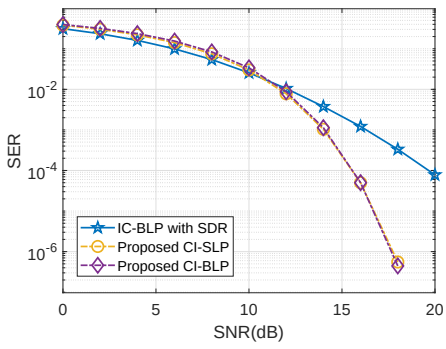

Fig. 9. SER performance, $N = 10$, $K_{\mathrm{u}} = 3$, $\Gamma = 4$dB, $p_0 = 30$dBm, QPSK.

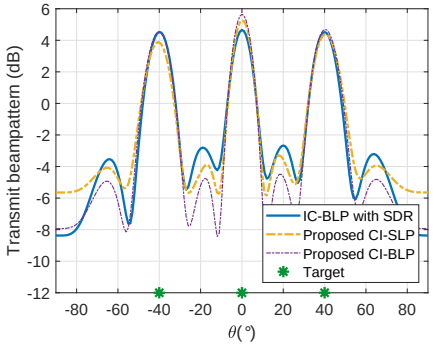

Fig. 10. Transmit beampatterns, $N = 10$, $K_{\mathrm{u}} = 3$, $K_{\mathrm{t}} = 3$, $\Gamma = 4$dB, $p_0 = 30$dBm, QPSK.

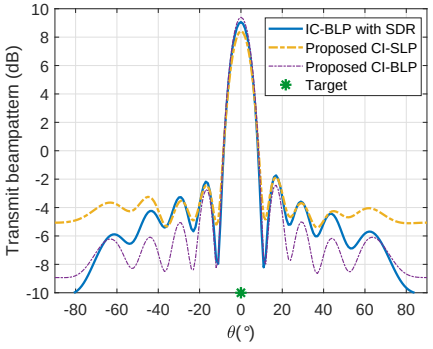

Fig. 11. Transmit beampatterns, $N = 10$, $K_{\mathrm{u}} = 3$, $K_{\mathrm{t}} = 1$, $\Gamma = 4$dB, $p_0 = 30$dBm, QPSK.

schemes. This means that the proposed schemes based on target illumination power are more flexible and stable for providing satisfactory beampatterns.

B. Simulation Results under Per-Antenna Power Constraint

Fig. 9 depicts the SER performance of different schemes under per-antenna power constraint when $N = 10$ and $K_{\mathrm{u}} = 3$. Compared with the SER results under the total power constraint shown in Fig. 3, we notice that the SER results of the CI-based precoding scheme remain unchanged under the per-antenna power constraint, which verifies the effectiveness of the proposed algorithm under the per-antenna power constraint. However, at this time, the SER results of the IC-BLP with SDR scheme deteriorate. This is because the conventional BLP design is based on the ideal assumption that the block length is sufficiently long. In the simulation, we consider the more practical case with finite-length blocks, where the IC-BLP with SDR scheme inevitably suffers performance loss.

Fig. 10 depicts the transmit beampatterns of different schemes under per-antenna power constraint with multiple targets. Fig. 11 depicts the transmit beampatterns of different schemes under per-antenna power constraint with a single target. It can be seen from Fig. 10 and Fig. 11 that the transmit beampattern of the CI-BLP scheme proposed in this paper is still the best, in terms of the mainlobe and the sidelobe. Compared with the transmit beampattern under the total power constraint in Fig. 4 and Fig. 5, under the per-antenna power constraint, the transmit beampatterns of all precoding schemes deteriorates, among which the transmit beampattern of CI-SLP scheme deteriorates more significantly. This is because the per-antenna power constraint is more stringent than the total power constraint, however.

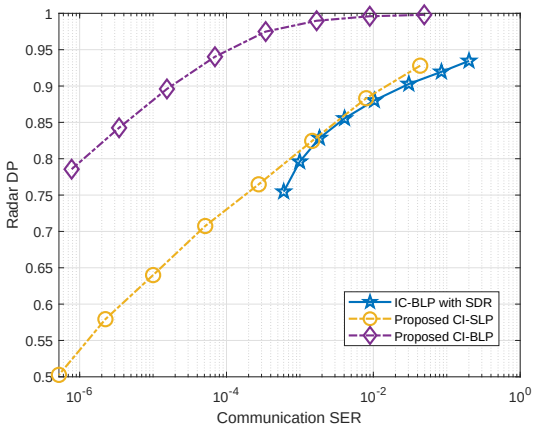

Fig. 12. Tradeoff between the communication SER and radar DP, $N = 10$, $K_{\mathrm{u}} = 3$, $K_{\mathrm{t}} = 1$, SNR $= 15$dB, SNRr $= 10$dBm, $p_0 = 30$dBm, QPSK.

Fig. 12 plots the trade-off between communication SER and radar sensing DP for different schemes under per-antenna power constraint. The communication SINR threshold Γ varies from 1dB to 8dB. We set SNR $= 15$dB for the SER calculation and SNRr $= 10$dBm for the DP calculation. At the same SER performance, the DP results of all schemes deteriorated under the per-antenna power constraint, compared with the total power constraint. It can be seen that the ISAC performance of the CI-SLP scheme deteriorates severely, while the BLP scheme, especially the CI-BLP scheme, is relatively less affected. This benefits from the fact that BLP schemes can optimize the intra-block power allocation to compensate for the performance loss due to more stringent power constraint. In Fig. 12, the communication performance loss of the IC-BLP with SDR scheme is significant. This is because we consider the more practical case with finite-length blocks in the simulation, where the performance loss caused by the per-antenna power constraint within each block is inevitable.

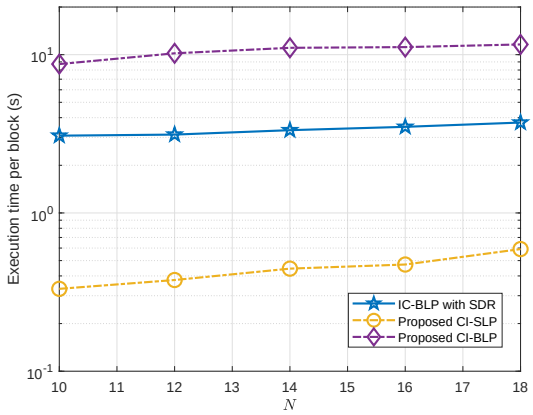

Fig. 13. Execution time of different schemes, $K_{\mathrm{u}} = 3$, $K_{\mathrm{t}} = 1$, $\Gamma = 4$dB, $p_0 = 30$dBm, QPSK.

Fig. 13 depicts the complexity of different schemes in terms of the execution time under per-antenna power constraint. As can be seen, the execution time of all schemes under the per-antenna power constraint is longer than that under the total power constraint, because the optimization problem becomes more complex. The execution time of CI-SLP is still less than that of CI-BLP. The execution time of the IC-BLP with SDR scheme does not change significantly, because different power constraints have little effect on the execution time of SDR.

VI. Conclusions

In this paper, we propose the CI-based precoding methods for MIMO ISAC systems from a uniform viewpoint for precoding with symbol level and block level. The illumination power of radar is maximized under communication CI constraint for ISAC performance enhancement. Specifically, the SCA and efficient algorithms are respectively designed for different power constraints. The simulation results show that the proposed CI-BLP scheme has significant advantages, compared with CI-SLP schemes in ISAC system considering the relaxed power allocation in a block level. While the computational complexity of CI-SLP is lower than that of CI-BLP because of the smaller size of the optimization problem. This indicates that the choice of CI-SLP and CI-BLP depends on the trade-off between performance and complexity in practical ISAC systems. Motivated by this work, more complicated ISAC CI-BLP schemes deserve further investigation. In addition to the target illumination power, this study can expand

to incorporate alternative radar metrics. These metrics may include beampattern squared error, the Cramer-Rao bound, and mutual information. Such exploration could yield further insights into the performance enhancements in ISAC systems with the aid of CI-BLP.

APPENDIX A
PROOF FOR $\nu > 0$

Assuming $\nu = 0$, $\boldsymbol{\mu}$ must satisfy (29a), as follows

$$\tilde{\mathbf{M}}^{\mathrm{T}}\boldsymbol{\mu} = \mathbf{d}. \tag{60}$$

Based on the constructions of $\tilde{\mathbf{M}}$ and $\mathbf{d}$, we know that the matrix $\tilde{\mathbf{M}}$ depends on the channel between the ISAC BS and users while the vector $\mathbf{d}$ depends on the target directions and the result obtained in the previous iteration. Hence, $\mathbf{d}$ is linearly independent with the columns in $\tilde{\mathbf{M}}^{\mathrm{T}}$ in practice considering the unrelated users and targets. Then considering $N \geq K_{\mathrm{u}}$, we have

$$\begin{aligned} &\operatorname{rank}\left(\tilde{\mathbf{M}}^{\mathrm{T}}\right) = \min\left\{2LN, 2LK_{\mathrm{u}}\right\} = 2LK_{\mathrm{u}}, \\ &\operatorname{rank}\left(\begin{bmatrix}\tilde{\mathbf{M}}^{\mathrm{T}} & \mathbf{d}\end{bmatrix}\right) = \min\left\{2LN, 2LK_{\mathrm{u}}+1\right\} = 2LK_{\mathrm{u}}+1, \end{aligned} \tag{61}$$

which means there is no solution for $\boldsymbol{\mu}$. Thus we can obtain $\nu > 0$, which completes the proof.

APPENDIX B
ANALYSIS OF PROBLEM $\mathcal{P}_3^{\mathrm{PAPC}}$

The Lagrangian dual function of $\mathcal{P}_3^{\mathrm{PAPC}}$ is given as below

$$\begin{aligned} \mathcal{L}\left(\tilde{\mathbf{x}}_{\mathrm{E}}, \boldsymbol{\mu}, \boldsymbol{\nu}\right) =& \mathbf{d}^{\mathrm{T}}\tilde{\mathbf{x}}_{\mathrm{E}} + \boldsymbol{\mu}^{\mathrm{T}}\left(t\cdot\mathbf{1} - \tilde{\mathbf{M}}\tilde{\mathbf{x}}_{\mathrm{E}}\right) \\ &+ \sum_{n=1}^{N}\nu_n\left(\tilde{\mathbf{x}}_{\mathrm{E}}^{\mathrm{T}}\tilde{\mathbf{E}}_n\tilde{\mathbf{x}}_{\mathrm{E}} - \frac{Lp_0}{N}\right), \end{aligned} \tag{62}$$

where $\boldsymbol{\mu} \in \mathbb{R}^{2LK_{\mathrm{u}}\times 1}$ and $\boldsymbol{\nu} \in \mathbb{R}^{N\times 1}$ are the non-negative dual variables. The KKT conditions for the optimality of $\mathcal{P}_3^{\mathrm{PAPC}}$ are expressed as follows.

$$\frac{\partial\mathcal{L}}{\partial\tilde{\mathbf{x}}_{\mathrm{E}}} = \mathbf{d} - \tilde{\mathbf{M}}^{\mathrm{T}}\boldsymbol{\mu} + 2\sum_{n=1}^{N}\nu_n\tilde{\mathbf{E}}_n\tilde{\mathbf{x}}_{\mathrm{E}} = 0, \tag{63a}$$

$$\boldsymbol{\mu}^{\mathrm{T}}\left(t\cdot\mathbf{1} - \tilde{\mathbf{M}}\tilde{\mathbf{x}}_{\mathrm{E}}\right) = 0,\ \mu_k \geq 0,\ \forall k \leq 2K_{\mathrm{u}}, \tag{63b}$$

$$\nu_n\left(\tilde{\mathbf{x}}_{\mathrm{E}}^{\mathrm{T}}\tilde{\mathbf{E}}_n\tilde{\mathbf{x}}_{\mathrm{E}} - \frac{Lp_0}{N}\right) = 0,\ \nu_n \geq 0,\ \forall n \in \mathcal{N}. \tag{63c}$$

Based on (63a), we can obtain:

$$2\sum_{n=1}^{N}\nu_n\tilde{\mathbf{E}}_n\tilde{\mathbf{x}}_{\mathrm{E}} = \tilde{\mathbf{M}}^{\mathrm{T}}\boldsymbol{\mu} - \mathbf{d}. \tag{64}$$

It is important to note that there exists the possibility that $\nu_n = 0$ for $n \in \mathcal{N}$ and thus $\sum_{n=1}^{N}\nu_n\tilde{\mathbf{E}}_n$ may be a rank-deficient matrix. In this case, it is difficult to obtain an optimal closed-form structure for $\tilde{\mathbf{x}}_{\mathrm{E}}$. This also means that it is challenging to get a simple form of the dual problem of $\mathcal{P}_3^{\mathrm{PAPC}}$, and therefore $\mathcal{P}_3^{\mathrm{PAPC}}$ can not be solved by the efficient algorithm proposed in Section III-D under total power constraint.

REFERENCES

[1] K. V. Mishra, M. Bhavani Shankar, V. Koivunen, B. Ottersten, and S. A. Vorobyov, "Toward Millimeter-Wave Joint Radar Communications: A Signal Processing Perspective," *IEEE Signal Process. Mag.*, vol. 36, no. 5, pp. 100–114, 2019.

[2] D. Ma, N. Shlezinger, T. Huang, Y. Liu, and Y. C. Eldar, "Joint Radar-Communication Strategies for Autonomous Vehicles: Combining Two Key Automotive Technologies," *IEEE Signal Process. Mag.*, vol. 37, no. 4, pp. 85–97, 2020.

[3] J. A. Zhang, F. Liu, C. Masouros, R. W. Heath, Z. Feng, L. Zheng, and A. Petropulu, "An Overview of Signal Processing Techniques for Joint Communication and Radar Sensing," *IEEE J. Sel. Topics Signal Process.*, vol. 15, no. 6, pp. 1295–1315, 2021.

[4] L. Zheng, M. Lops, Y. C. Eldar, and X. Wang, "Radar and Communication Coexistence: An Overview: A Review of Recent Methods," *IEEE Signal Process. Mag.*, vol. 36, no. 5, pp. 85–99, 2019.

[5] N. C. Luong, X. Lu, D. T. Hoang, D. Niyato, and D. I. Kim, "Radio Resource Management in Joint Radar and Communication: A Comprehensive Survey," *IEEE Commun. Surveys Tuts.*, vol. 23, no. 2, pp. 780–814, 2021.

[6] J. A. Zhang, M. L. Rahman, K. Wu, X. Huang, Y. J. Guo, S. Chen, and J. Yuan, "Enabling Joint Communication and Radar Sensing in Mobile NetworksA Survey," *IEEE Commun. Surveys Tuts.*, vol. 24, no. 1, pp. 306–345, 2022.

[7] F. Liu, Y. Cui, C. Masouros, J. Xu, T. X. Han, Y. C. Eldar, and S. Buzzi, "Integrated Sensing and Communications: Toward Dual-Functional Wireless Networks for 6G and Beyond," *IEEE J. Sel. Areas Commun.*, vol. 40, no. 6, pp. 1728–1767, 2022.

[8] J. Qian, M. Lops, L. Zheng, X. Wang, and Z. He, "Joint System Design for Coexistence of MIMO Radar and MIMO Communication," *IEEE Trans. Signal Process.*, vol. 66, no. 13, pp. 3504–3519, 2018.

[9] B. Tang, H. Wang, L. Qin, and L. Li, "Waveform Design for Dual-function MIMO Radar-communication Systems," in *2020 IEEE 11th Sensor Array and Multichannel Signal Processing Workshop (SAM)*, Hangzhou, China, 2020, pp. 1–5.

[10] X. Liu, T. Huang, N. Shlezinger, Y. Liu, J. Zhou, and Y. C. Eldar, "Joint Transmit Beamforming for Multiuser MIMO Communications and MIMO Radar," *IEEE Trans. Signal Process.*, vol. 68, pp. 3929–3944, 2020.

[11] F. Liu, C. Masouros, A. Li, H. Sun, and L. Hanzo, "MU-MIMO Communications With MIMO Radar: From Co-Existence to Joint Transmission," *IEEE Trans. Wireless Commun.*, vol. 17, no. 4, pp. 2755–2770, 2018.

[12] P. Kumari, S. A. Vorobyov, and R. W. Heath, "Adaptive Virtual Waveform Design for Millimeter-Wave Joint CommunicationRadar," *IEEE Trans. Signal Process.*, vol. 68, pp. 715–730, 2020.

[13] X. Hu, C. Masouros, F. Liu, and R. Nissel, "MIMO-OFDM dual-functional radar-communication systems: Low-PAPR waveform design," 2021. [Online]. Available: https://arxiv.org/abs/2109.13148.

[14] C. Xu, B. Clerckx, and J. Zhang, "Multi-Antenna Joint Radar and Communications: Precoder Optimization and Weighted Sum-Rate vs Probing Power Tradeoff," *IEEE Access*, vol. 8, pp. 173 974–173 982, 2020.

[15] X. Hu, C. Masouros, F. Liu, and R. Nissel, "Low-PAPR DFRC MIMO-OFDM Waveform Design for Integrated Sensing and Communications," in *ICC 2022 - IEEE International Conference on Communications*, 2022, pp. 1599–1604.

[16] C. Masouros, T. Ratnarajah, M. Sellathurai, C. B. Papadias, and A. K. Shukla, "Known Interference in the Cellular Downlink: A Performance Limiting Factor or a Source of Green Signal Power?" *IEEE Commun. Mag.*, vol. 51, no. 10, pp. 162–171, Oct. 2013.

[17] M. Alodeh, S. Chatzinotas, and B. Ottersten, "Constructive Multiuser Interference in Symbol Level Precoding for the MISO Downlink Channel," *IEEE Trans. Sig. Process.*, vol. 63, no. 9, pp. 2239–2252, May 2015.

[18] C. Masouros and G. Zheng, "Exploiting Known Interference as Green Signal Power for Downlink Beamforming Optimization," *IEEE Trans. Signal Process.*, vol. 63, no. 14, pp. 3628–3640, 2015.

[19] M. Alodeh, S. Chatzinotas, and B. Ottersten, "Energy-Efficient Symbol-Level Precoding in Multiuser MISO Based on Relaxed Detection Region," *IEEE Trans. Wireless Commun.*, vol. 15, no. 5, pp. 3755–3767, May 2016.

[20] M. Alodeh, S. Chatzinotas, and B. Ottersten, "Symbol-Level Multiuser MISO Precoding for Multi-Level Adaptive Modulation," *IEEE Trans. Wireless Commun.*, vol. 16, no. 8, pp. 5511–5524, Aug. 2017.

[21] C. Masouros and E. Alsusa, "Dynamic linear precoding for the exploitation of known interference in MIMO broadcast systems," *IEEE Trans. Wireless Commun.*, vol. 8, no. 3, pp. 1396–1404, 2009.

[22] M. Alodeh, D. Spano, A. Kalantari, C. G. Tsinos, D. Christopoulos, S. Chatzinotas, and B. Ottersten, "Symbol-Level and Multicast Precoding for Multiuser Multiantenna Downlink: A State-of-the-Art, Classification, and Challenges," *IEEE Commun. Surveys Tuts.*, vol. 20, no. 3, pp. 1733–1757, 2018.

[23] A. Li, D. Spano, J. Krivochiza, S. Domouchtsidis, C. G. Tsinos, C. Masouros, S. Chatzinotas, Y. Li, B. Vucetic, and B. Ottersten, "A Tutorial on Interference Exploitation via Symbol-Level Precoding: Overview, State-of-the-Art and Future Directions," *IEEE Commun. Surveys Tuts.*, vol. 22, no. 2, pp. 796–839, Mar. 2020.

[24] R. Liu, M. Li, Q. Liu, and A. L. Swindlehurst, "Dual-Functional Radar-Communication Waveform Design: A Symbol-Level Precoding Approach," *IEEE J. Sel. Topics Signal Process.*, vol. 15, no. 6, pp. 1316–1331, 2021.

[25] R. Liu, M. Li, Q. Liu, and A. L. Swindlehurst, "Joint Waveform and Filter Designs for STAP-SLP-Based MIMO-DFRC Systems," *IEEE J. Sel. Areas Commun.*, vol. 40, no. 6, pp. 1918–1931, 2022.

[26] Z. Liao, F. Liu, A. Li, and C. Masouros, "Faster-Than-Nyquist Symbol-Level Precoding for Wideband Integrated Sensing and Communications," *IEEE Trans. Wireless Commun.*, vol. 23, no. 8, pp. 10 445–10 458, 2024.

[27] P. Li, M. Li, R. Liu, Q. Liu, and A. Lee Swindlehurst, "MIMO-OFDM ISAC Waveform Design for Range-Doppler Sidelobe Suppression," *IEEE Trans. Wireless Commun.*, vol. 24, no. 2, pp. 1001–1015, 2025.

[28] P. Jiang, M. Li, R. Liu, W. Wang, and Q. Liu, "SLP-Based Dual-Functional Waveform Design for ISAC Systems: A Deep Learning Approach," *IEEE Trans. Veh. Technol.*, pp. 1–15, 2025.

[29] Y. Wang, X. Hu, A. Li, C. Masouros, K.-K. Wong, and K. Yang, "Symbol-Scaling Based Interference Exploitation in ISAC Systems: From Symbol Level to Block Level," *IEEE Trans. Wireless Commun.*, vol. 24, no. 3, pp. 2451–2466, 2025.

[30] A. Li, C. Shen, X. Liao, C. Masouros, and A. L. Swindlehurst, "Practical Interference Exploitation Precoding Without Symbol-by-Symbol Optimization: A Block-Level Approach," *IEEE Trans. Wireless Commun.*, vol. 22, no. 6, pp. 3982–3996, 2023.

[31] Y. Wang, Y. Wen, A. Li, X. Hu, and C. Masouros, "Block-Level Interference Exploitation Precoding for MU-MISO: An ADMM Approach," *IEEE Trans. Commun.*, pp. 1–1, 2024.

[32] Hao, Neely, and J. Michael, "A Simple Parallel Algorithm with an O(1/t) Convergence Rate for General Convex Programs," *SIAM Journal on Optimization: A Publication of the Society for Industrial and Applied Mathematics*, 2017.

[33] S. Boyd, N. Parikh, E. Chu, B. Peleato, and J. Eckstein, *Distributed Optimization and Statistical Learning via the Alternating Direction Method of Multipliers*, 2011.

[34] P. Stoica, J. Li, and Y. Xie, "On Probing Signal Design For MIMO Radar," *IEEE Trans. Signal Process.*, vol. 55, no. 8, pp. 4151–4161, 2007.

[35] L. Wu, B. Wang, Z. Cheng, B. S. M. R, and B. Ottersten, "Joint Symbol-Level Precoding and Sub-Block-Level RIS Design for Dual-Function Radar-Communications," in *2023 IEEE International Conference on Acoustics, Speech and Signal Processing (ICASSP)*, Rhodes Island, Greece, 2023, pp. 1–5.

[36] A. Li, C. Masouros, B. Vucetic, Y. Li, and A. L. Swindlehurst, "Interference Exploitation Precoding for Multi-Level Modulations: Closed-Form Solutions," *IEEE Trans. Commun.*, vol. 69, no. 1, pp. 291–308, 2021.

[37] A. Li, C. Masouros, F. Liu, and A. L. Swindlehurst, "Massive MIMO 1-Bit DAC Transmission: A Low-Complexity Symbol Scaling Approach," *IEEE Trans. Wireless Commun.*, vol. 17, no. 11, pp. 7559–7575, Nov. 2018.

[38] S. Boyd and L. Vandenberghe, *Convex Optimization*. Cambridge University Press, 2004.

[39] R. Liu, M. Li, Q. Liu, and A. L. Swindlehurst, "Secure Symbol-Level Precoding in MU-MISO Wiretap Systems," *IEEE Trans. Information Forensics and Security*, vol. 15, pp. 3359–3373, 2020.

[40] K.-Y. Wang, A. M.-C. So, T.-H. Chang, W.-K. Ma, and C.-Y. Chi, "Outage Constrained Robust Transmit Optimization for Multiuser MISO Downlinks: Tractable Approximations by Conic Optimization," *IEEE Trans. Signal Process.*, vol. 62, no. 21, pp. 5690–5705, 2014.

[41] F. Liu, L. Zhou, C. Masouros, A. Li, W. Luo, and A. Petropulu, "Toward Dual-functional Radar-Communication Systems: Optimal Waveform Design," *IEEE Trans. Signal Process.*, vol. 66, no. 16, pp. 4264–4279, 2018.

[42] Y. Wen, H. Wang, A. Li, X. Liao, and C. Masouros, "Low-Complexity Interference Exploitation MISO Precoding Under Per-Antenna Power Constraint," *IEEE Trans. Wireless Commun.*, vol. 23, no. 8, pp. 9943–9957, 2024.

[43] Y. Wen, J. Yang, A. Li, X. Liao, and C. Masouros, "Parallel Solution for Per-Antenna Power Constrained Symbol-Level MU-MISO Precoding," *IEEE Trans. Commun.*, pp. 1–1, 2025.

[44] D. P. Bertsekas, "Nonlinear Programming: 2nd edition," 1999.

[45] A. Khawar, A. Abdelhadi, and C. Clancy, "Target detection performance of spectrum sharing mimo radars," *IEEE Sensors Journal*, vol. 15, no. 9, pp. 4928–4940, 2015.

ISAC Enhancement with Interference Exploitation: From A Uniform Viewpoint for Symbol Level and Block Level

by Yiran Wang, Xiaoyan Hu, Ang Li, Christos Masouros, Kai-Kit Wong, and Kun Yang

Response to the Reviewers' Comments

Dear Editor and Reviewers,

Motivated by the comments from the Reviewers in the previous submission, we have further revised the manuscript (Paper ID: *VT- 2025-02669*, Title: *ISAC Enhancement with Interference Exploitation: From A Uniform Viewpoint for Symbol Level and Block Level*), and hereby resubmit the above manuscript for consideration for future publication in the *IEEE Transactions on Vehicular Technology*.

We would like to thank the Editor and Reviewers for their supportive comments and constructive remarks, which have all been carefully considered to further enhance the readability and quality of this manuscript. For clarity, we first summarize the major revisions in the resubmitted paper as per the Reviewers' comments:

1. Recommended by Reviewer 1 and Reviewer 3, we have provided some references to support the research on per-antenna power constraints at the beginning of Section IV. Recommended by Reviewer 2, we have reviewed the latest CI-SLP designs in ISAC systems and summarized them in the Introduction.
2. Recommended by Reviewer 2 and Reviewer 3, we have provided some description of the Hooke-Jeeves pattern search algorithm in Section III-D of this paper.

3. Recommended by Reviewer 1 and Reviewer 2, we have provided a detailed explanation of the rank computation in Eq. (61) in the revised version.

Below is the list of all the modifications made as per the Reviewers' recommendations. All alterations made due to the comments are in blue lettering in the revised manuscript to ease further revision. Within this report, the Reviewers' comments appear in *italic* form, and our responses are interleaved in plain text.

Sincerely,

The Authors

Reviewer 1:

Reviewer: *This paper proposes the CI-SLP and CI-BLP designs for ISAC systems and designs efficient algorithms for precoding schemes under total power constraints and per-antenna power constraints, respectively. The simulation results show that CI-BLP has a more significant performance advantage compared to CI-SLP, especially under per-antenna power constraints. The motivation of this paper is clear, and the structure is well-organized. The reviewer has the following comments.*

Authors: We thank the Reviewer for the summary of our work and the positive comments. Below we address your remaining concerns one by one.

(1) **Reviewer:** *Fig. 1 only represents a specific case for a particular user. Can the optimization problem formulated in the paper guarantee that the symbol of each user is pushed away from its decision boundaries?*

Authors: Regarding the Reviewer's concern, we kindly note that it is true that the optimization problem formulated in the paper can guarantee that the symbol of each user is pushed away from its decision boundaries. This is because, by constraining all CI scaling factors, we can guarantee that the noise-free received signal of each user remains at least a prescribed distance away from both of its decision boundaries. As an illustrative example, below we depict the constellation diagram of the proposed ISAC CI-BLP scheme under QPSK modulation, including the received signals of all users.

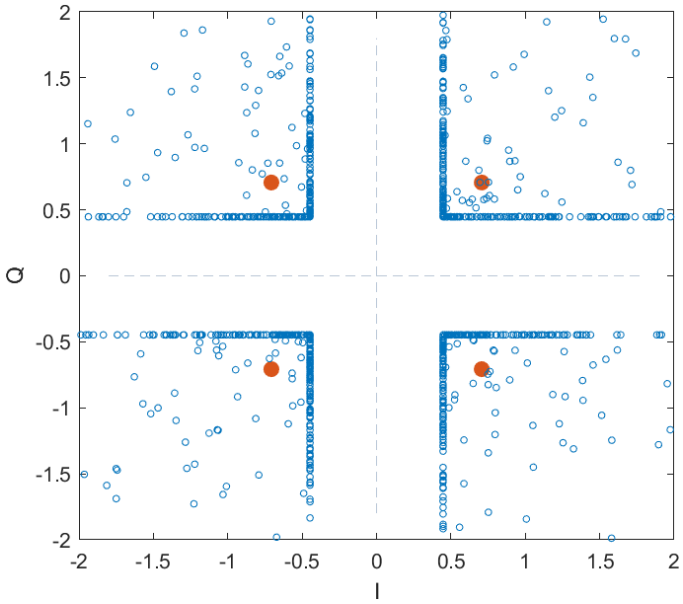

Fig. A Constellation diagram of the proposed ISAC CI-BLP scheme, $N = 10$, $K_{\mathrm{u}} = 3$, $K_{\mathrm{t}} = 3$, $\Gamma = 4\mathrm{dB}$, $L = 6$, QPSK.

In Fig. A, solid red circles represent nominal constellation points, hollow blue circles represent received signals, and dashed lines represent decision boundaries. It can be seen that the received signals of all users are pushed away from their decision boundaries and thus fall into the constructive region.

(2) **Reviewer:** *This paper contributes to the uniform viewpoint for ISAC precoding scheme for symbol level and block level. Please explain the uniform policy.*

Authors: Regarding the Reviewer's concern on the uniform policy, firstly, conventional block-level ISAC precoding schemes optimize the second-order statistics of the transmit signal under the assumption of a large number of samples, whereas symbol-level ISAC precoding schemes exploit instantaneous data symbols and CSI to optimize the transmit signal slot-by-slot based on CI. Consequently, the two families differ in design philosophy and performance metrics. To enable a fair comparison, we

propose a CI-based block-level ISAC precoding scheme which shares identical performance metrics with symbol-level ISAC precoding scheme. Leveraging a matrix-based formulation, we further derive a unified problem description that encompasses both symbol-level and block-level schemes. This unified framework allows us to compare the ISAC performance of symbol-level and block-level precoding schemes under various power constraints from a unified perspective.

(3) **Reviewer:** *The authors should provide more references to illustrate the application of per-antenna power constraints in practical systems.*

Authors: We thank the Reviewer for the valuable suggestion regarding the references. Most existing works on precoding consider the total power constraint, while in practical systems, each transmit antenna is usually equipped with its dedicated power amplifier. Therefore, it is more realistic to design precoding approaches that incorporate the per-antenna power constraint. In [R1], the authors investigate the conventional block-level precoding under the per-antenna power constraint in ISAC systems, while in [R2] and [R3], the authors focus on symbol-level precoding design under the per-antenna power constraint in communication-only systems.

In this revision, we have included the relevant references and added the following statement at the beginning of Section IV:

"In practical systems, each transmit antenna is usually equipped with its dedicated power amplifier. Therefore, it is more realistic to design ISAC precoding approaches that incorporate the per-antenna power constraint [41]-[43]. In this section we design the transmit ISAC waveform matrix **X** under per-antenna power constraint."

[R1] F. Liu, L. Zhou, C. Masouros, A. Li, W. Luo, and A. Petropulu, "Toward Dual-functional

Radar-Communication Systems: Optimal Waveform Design," IEEE Trans. Signal Process., vol. 66, no. 16, pp. 4264–4279, 2018.

[R2] Y. Wen, H. Wang, A. Li, X. Liao, and C. Masouros, "Low-Complexity Interference Exploitation MISO Precoding Under Per-Antenna Power Constraint," IEEE Trans. Wireless Commun., vol. 23, no. 8, pp. 9943–9957, 2024.

[R3] Y. Wen, J. Yang, A. Li, X. Liao, and C. Masouros, "Parallel Solution for Per-Antenna Power Constrained Symbol-Level MU-MISO Precoding," IEEE Trans. Commun., pp. 1–1, 2025.

(4) **Reviewer:** *The reviewer suggests that providing the dimensions of the variables in Eq. 22 and Eq. 23 would enhance the readability of the paper.*

Authors: We thank the Reviewer for the valuable suggestion on improving the readability of our paper. In Eq. (22) and Eq. (23), we have $\tilde{\mathbf{x}}_{\mathrm{E}} \in \mathbb{R}^{2\mathrm{LN}\times 1}$, $\widetilde{\mathbf{D}} \in \mathbb{R}^{2LN\times 2LN}$ and $\widetilde{\mathbf{M}} \in \mathbb{R}^{2LK_u\times 2LN}$.

In this version, we have revised the statement above Eq. (22) and Eq. (23) as follows:

"… where $\tilde{\mathbf{x}}_{\mathrm{E}} \in \mathbb{R}^{2\mathrm{LN}\times 1}$, $\widetilde{\mathbf{D}} \in \mathbb{R}^{2LN\times 2LN}$ and $\widetilde{\mathbf{M}} \in \mathbb{R}^{2LK_u\times 2LN}$ are respectively defined as: …"

(5) **Reviewer:** *The authors should add a description of the function* Π *in Eq. 58.*

Authors: We thank the Reviewer for the valuable suggestion on improving the readability of our paper. In Eq. (58), $\Pi_{\mathcal{X}}(\cdot)$ is a projection operator, and $\Pi_{\mathcal{X}}(\hat{\mathbf{z}})$ denotes the projection of the vector $\hat{\mathbf{z}}$ onto the set $\mathcal{X}$.

In this version, we have revised the statement below Eq. (58) into

"… where $\Pi_{\mathcal{X}}(\cdot)$ is a projection operator, and $\Pi_{\mathcal{X}}(\hat{\mathbf{z}})$ denotes the projection of the vector $\hat{\mathbf{z}}$ onto the set $\mathcal{X}$. For any $\hat{\mathbf{z}} \in \mathbb{R}^{2LN\times 1}$, $\Pi_{\mathcal{X}}(\hat{\mathbf{z}})$ can be implemented in a closed form as (59) on the top of the next page."

(6) **Reviewer:** *The authors should provide the method for calculating the rank in Equation (61).*

Authors: We thank the Reviewer for the careful reading of our paper. In Eq. (60), based on the constructions of $\widetilde{\mathbf{M}}$ and $\mathbf{d}$, we know that the matrix $\widetilde{\mathbf{M}}$ depends on the channel between the ISAC BS and users while the vector $\mathbf{d}$ depends on the target directions and the result obtained in the previous iteration. Hence, $\mathbf{d}$ is linearly independent with the columns in $\widetilde{\mathbf{M}}^{\mathrm{T}}$ in practice considering the unrelated users and targets. Then considering $N \geq K_{\mathrm{u}}$, we can obtain the rank in Eq. (61) of this paper.

In this revision, we have included the statement below Eq. (60) as follows:

"Based on the constructions of $\widetilde{\mathbf{M}}$ and $\mathbf{d}$, we know that the matrix $\widetilde{\mathbf{M}}$ depends on the channel between the ISAC BS and users while the vector $\mathbf{d}$ depends on the target directions and the result obtained in the previous iteration. Hence, $\mathbf{d}$ is linearly independent with the columns in $\widetilde{\mathbf{M}}^{\mathrm{T}}$ in practice considering the unrelated users and targets. Then considering $N \geq K_{\mathrm{u}}$, we have

$$\mathrm{rank}\left(\widetilde{\mathbf{M}}^{\mathrm{T}}\right) = \min\{2LN, 2LK_{\mathrm{u}}\} = 2LK_{\mathrm{u}},$$

$$\mathrm{rank}\left(\left[\widetilde{\mathbf{M}}^{\mathrm{T}} \quad \mathbf{d}\right]\right) = \min\{2LN, 2LK_{\mathrm{u}} + 1\} = 2LK_{\mathrm{u}} + 1,$$

which means there is no solution for $\boldsymbol{\mu}$. …"

Reviewer 2:

Reviewer: *In this paper, the authors investigate the precoding scheme based on interference exploitation in ISAC systems. Building upon the CI-SLP scheme, the CI-BLP scheme is further proposed. Simulation results validate the advantages of the CI-based precoding schemes in terms of ISAC performance. This paper is generally well-written with novel ideas, and the reviewer has the following concerns.*

Authors: We thank the Reviewer for the summary of our work and the positive comments. Below we address your remaining concerns one by one.

(1) **Reviewer:** *It would be better if the authors could include more related work on CI-SLP in ISAC systems in the Introduction.*

Authors: We thank the Reviewer for the valuable suggestion. Besides [24] and [25] ([29] in this version), some other works also investigate CI-SLP design in ISAC systems. In [R4] (cited as [25] in the revised paper), the authors jointly optimize transmit signals and receive filters for MIMO-ISAC by leveraging space-time adaptive processing (STAP) and CI-SLP. In [R5] (cited as [26] in the revised paper), the authors extend the framework to wideband FTN-ISAC, formulating the corresponding CI-SLP problem under faster-than-Nyquist signaling. A CI-SLP design for OFDM-ISAC is proposed in [R6] (cited as [27] in the revised paper), where the range-Doppler integrated sidelobe level (ISL) of the ambiguity function is minimized while target illumination power, communication CI, and transmit power constraints are satisfied. Building on the ISAC paradigm presented in [24], a deep-learning-based framework is introduced in [R7] (cited as [28] in the revised paper) to enable low-complexity CI-SLP implementation. Nevertheless, this scheme exhibits a modest performance loss compared with the scheme in [24].

Following the Reviewer's suggestion, we have further included these works in our paper and added the statement in Paragraph 4 of the Introduction as follows:

"… However, due to the complicated processing of quartic function in the optimization objective and the need for thousands of iterations, the computational complexity of this scheme is too high to be accepted in practical systems. In [25], the authors jointly optimize transmit signals and receive filters for MIMO-ISAC by leveraging space-time adaptive processing (STAP) and CI-SLP. In [26], the authors extend the framework to wideband FTN-ISAC, formulating the corresponding CI-SLP problem under faster-than-Nyquist signaling. A CI-SLP design for OFDM-ISAC is proposed in [27], where the range-Doppler integrated sidelobe level (ISL) of the ambiguity function is minimized while target illumination power, communication CI, and transmit power constraints are satisfied. Building on the ISAC paradigm presented in [24], a deep-learning-based framework is introduced in [28] to enable low-complexity CI-SLP implementation. Nevertheless, this scheme exhibits a modest performance loss compared with the scheme in [24]. In [29], a low-complexity CI-SLP scheme based on communication CI and radar illumination power is proposed. …"

[R4] R. Liu, M. Li, Q. Liu, and A. L. Swindlehurst, "Joint Waveform and Filter Designs for STAP-SLP-Based MIMO-DFRC Systems," IEEE J. Sel. Areas Commun., vol. 40, no. 6, pp. 1918–1931, 2022.

[R5] Z. Liao, F. Liu, A. Li, and C. Masouros, "Faster-Than-Nyquist Symbol-Level Precoding for Wideband Integrated Sensing and Communications," IEEE Trans. Wireless Commun., vol. 23, no. 8, pp. 10 445–10 458, 2024.

[R6] P. Li, M. Li, R. Liu, Q. Liu, and A. Lee Swindlehurst, "MIMO-OFDM ISAC Waveform Design for Range-Doppler Sidelobe Suppression," IEEE Trans. Wireless Commun., vol. 24, no. 2, pp. 1001–1015, 2025.

[R7] P. Jiang, M. Li, R. Liu, W. Wang, and Q. Liu, "SLP-Based Dual-Functional Waveform Design for ISAC Systems: A Deep Learning Approach," IEEE Trans. Veh. Technol., pp. 1–15, 2025.

(2) **Reviewer:** *The paper uses CI constraints to guarantee communication SER performance. Why not directly constrain the SER?*

Authors: We thank the Reviewer for the careful reading of our paper. Firstly, we adopt CI constraints because CI constraints guarantee that each noiseless received signal falls within the CI region and is pushed as far as possible from its corresponding decision boundaries. From the perspective of geometric analysis, CI constraints ensure a low average SER for the ISAC system. However, after a more in-depth literature review, we agree with the Reviewer that the CI constraints is not the exact SER expression, which may lead to a slightly degraded SER performance in some cases. For high-order QAM modulation in the communication-only system, [R8] gives the expression of SER with respect to the transmit signal and the rescaling factor based on the noise distribution, and constructs the optimization problem to minimize SER. Since the objective function based on the SER expression is not convex, alternate optimization, Riemannian manifold algorithm and gradient descent method are adopted to solve it. Simulation results show that for high-order QAM modulation, the SER of the scheme based on SER expression is better than that of the scheme based on CI, as expected. However, the complexity of this scheme is relatively high, especially when the number of transmit antennas is larger than the number of users.

In this paper, we strive to develop a low-complexity CI-SLP scheme for the multi-target ISAC system. Therefore, we hope the Reviewer condones our choice to adopt CI constraints, rather than directly constraining the SER, in the design of the ISAC precoding scheme.

[R8] Y. Wang, H. Hou, W. Wang, and X. Yi, "Symbol-Level Precoding for Average SER Minimization in Multiuser MISO Systems," IEEE Wireless Communications Letters, vol. 13, no. 4, pp. 1103–1107, 2024

(3) **Reviewer:** *The authors should provide some description of the utilized Hooke-Jeeves pattern search algorithm.*

Authors: We thank the Reviewer for the valuable suggestion. The Hooke-Jeeves pattern search algorithm is an iterative derivative-free method. At each iteration, we first probe the vector $\boldsymbol{\mu}$ along each dimension with a fixed step size to detect the most favorable descent direction. If no further improvement can be achieved, the step size is halved. It can be observed that the optimization problem in Eq. (37) has extremely simple constraints, which allows it to be solved by the Hooke-Jeeves pattern search algorithm with markedly reduced computational complexity.

In this revision, we have included the statement below Eq. (37) as follows:

"Note that the problem $\mathcal{P}_4^{\mathrm{TPC}}$ can be more efficiently solved than the problem $\mathcal{P}_3^{\mathrm{TPC}}$ via the Hooke-Jeeves pattern search algorithm [39]. The Hooke-Jeeves pattern search algorithm is an iterative derivative-free method. At each iteration, we first probe the vector $\boldsymbol{\mu}$ along each dimension with a fixed step size to detect the most favorable descent direction. If no further improvement can be achieved, the step size is halved. It can be observed that the problem $\mathcal{P}_4^{\mathrm{TPC}}$ has extremely simple constraints, which allows it to be solved by the Hooke-Jeeves pattern search algorithm with markedly reduced computational complexity. After solving the dual problem $\mathcal{P}_4^{\mathrm{TPC}}$, we can obtain $\boldsymbol{\mu}^*$ and then we can obtain $\tilde{\mathbf{x}}_{\mathrm{E}}^*$ of $\mathcal{P}_3^{\mathrm{TPC}}$ via (31)."

(4) **Reviewer:** *The simulation results show that the CI-BLP scheme has higher computational complexity. What are the advantages of the CI-BLP scheme over the CI-SLP scheme?*

Authors: Regarding the Reviewer's concern on the advantages of the CI-BLP scheme, the advantages of CI-BLP over CI-SLP are summarized as

follows:

1) Compared with the CI-SLP scheme that optimizes the transmit signals at the symbol level, the CI-BLP scheme considers a block of symbols and the optimization requires execution only once for each block, which can greatly reduce the update frequency of the transmit precoders.
2) CI-BLP scheme optimization enables block-level power allocation and further improves ISAC performance compared to CI-SLP scheme. This is because relaxed power constraint in CI-BLP optimization allows more freedom to power allocation among different symbol slots.
3) CI-BLP can be seen as a generalization of CI-SLP. The flexible tradeoff between ISAC performance and computational complexity can be achieved by modifying the length of the considered block. In other words, CI-BLP scheme can achieve better ISAC performance and lower update frequency than CI-SLP scheme if the computational complexity allows.

(5) **Reviewer:** *In Appendix A, directly providing the ranks of the matrices is not rigorous. The authors should supplement the detailed derivations of Eq. 61.*

Authors: We thank the Reviewer for the careful reading of our paper. In Eq. (60), based on the constructions of $\widetilde{\mathbf{M}}$ and $\mathbf{d}$, we know that the matrix $\widetilde{\mathbf{M}}$ depends on the channel between the ISAC BS and users while the vector $\mathbf{d}$ depends on the target directions and the result obtained in the previous iteration. Hence, $\mathbf{d}$ is linearly independent with the columns in $\widetilde{\mathbf{M}}^{\mathrm{T}}$ in practice considering the unrelated users and targets. Then considering $N \geq K_{\mathrm{u}}$, we can obtain the rank in Eq. (61) of this paper.

In this revision, we have included the statement below Eq. (60) as follows:

"Based on the constructions of $\widetilde{\mathbf{M}}$ and $\mathbf{d}$, we know that the matrix $\widetilde{\mathbf{M}}$ depends on the channel between the ISAC BS and users while the vector $\mathbf{d}$ depends on the target directions and the result obtained in the previous

iteration. Hence, $\mathbf{d}$ is linearly independent with the columns in $\widetilde{\mathbf{M}}^{\mathrm{T}}$ in practice considering the unrelated users and targets. Then considering $N \geq K_{\mathrm{u}}$, we have

$$\mathrm{rank}\left(\widetilde{\mathbf{M}}^{T}\right) = \min\{2LN, 2LK_{\mathrm{u}}\} = 2LK_{\mathrm{u}},$$

$$\mathrm{rank}\left(\left[\widetilde{\mathbf{M}}^{T} \quad \mathbf{d}\right]\right) = \min\{2LN, 2LK_{\mathrm{u}} + 1\} = 2LK_{\mathrm{u}} + 1,$$

which means there is no solution for $\boldsymbol{\mu}$. …"

(6) **Reviewer:** *The authors should provide additional descriptions of the matrix* $\widetilde{\mathbf{M}}$ *in Equation (23).*

Authors: We thank the Reviewer for the valuable suggestion on improving the readability of our paper. In Eq. (23), $\widetilde{\mathbf{M}}$ is a block diagonal matrix, with each diagonal block being the coefficient matrix $\mathbf{M}_l$ $(l \in \mathcal{L})$ corresponding to each time slot in the block.

In this revision, we have included the statement below Eq. (23) as follows:

"Here, $\otimes$ represents the Kronecker product and $\widetilde{\mathbf{M}}$ is a block diagonal matrix, with each diagonal block being the coefficient matrix $\mathbf{M}_l$ $(l \in \mathcal{L})$ corresponding to each time slot in the block."

(7) **Reviewer:** *The authors should provide the dimensions of the dual variables in Equations (28) and (62).*

Authors: We thank the Reviewer for the valuable suggestion on improving the readability of our paper. In Eq. (28), the dual variable $\boldsymbol{\mu} \in \mathbb{R}^{2LK_{\mathrm{u}} \times 1}$ and the dual variable υ is a scalar. In Eq. (62), the dual variable $\boldsymbol{\mu} \in \mathbb{R}^{2LK_{\mathrm{u}} \times 1}$ and the dual variable $\boldsymbol{\upsilon} \in \mathbb{R}^{N \times 1}$.

In this revision, we have updated the statement below Eq. (28) as

"… where $\boldsymbol{\mu} \in \mathbb{R}^{2LK_{\mathrm{u}} \times 1}$ and υ are non-negative dual variables

corresponding to inequality constraints (27a) and (27b), respectively. …”

and the statement below Eq. (62) as

“… where $\boldsymbol{\mu} \in \mathbb{R}^{2LK_{\mathrm{u}} \times 1}$ and $\boldsymbol{\nu} \in \mathbb{R}^{N \times 1}$ are the non-negative dual variables. …”

Reviewer 3:

Reviewer: *This paper proposes a novel precoding scheme for ISAC systems based on interference exploitation, which significantly improves the communication SER performance and target illumination power. The reviewer believes that the motivation and contributions of this paper are clear. However, before formal publication, the reviewer has the following suggestions.*

Authors: We thank the Reviewer for the summary of our work and the positive comments. Below we address your remaining concerns one by one.

(1) **Reviewer:** *This paper seems to only consider the QPSK modulation scheme. Can the proposed scheme be extended to higher-order modulation schemes?*

Authors: Regarding the Reviewer's concern on the modulation scheme, firstly, the proposed ISAC CI-BLP scheme can be easily extended to higher-order modulation schemes by tailoring the CI regions to the specific modulation scheme. As an example, for 8PSK modulation, the SER performance and transmit beampattern of the proposed ISAC CI-BLP scheme under the total-power constraint are presented below.

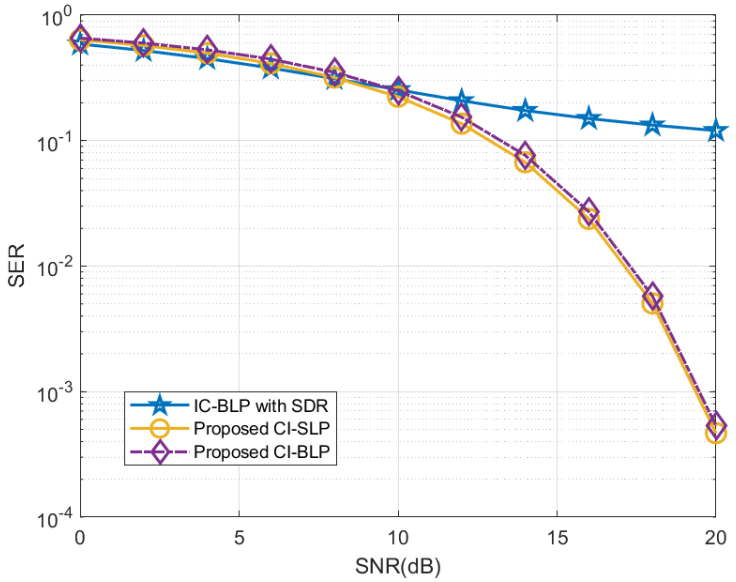

Fig. B SER performance, $N = 10$, $K_{\mathrm{u}} = 3$, $K_{\mathrm{t}} = 1$, $\Gamma = 4\mathrm{dB}$, $p_0 = 30\mathrm{dB}$, 8PSK.

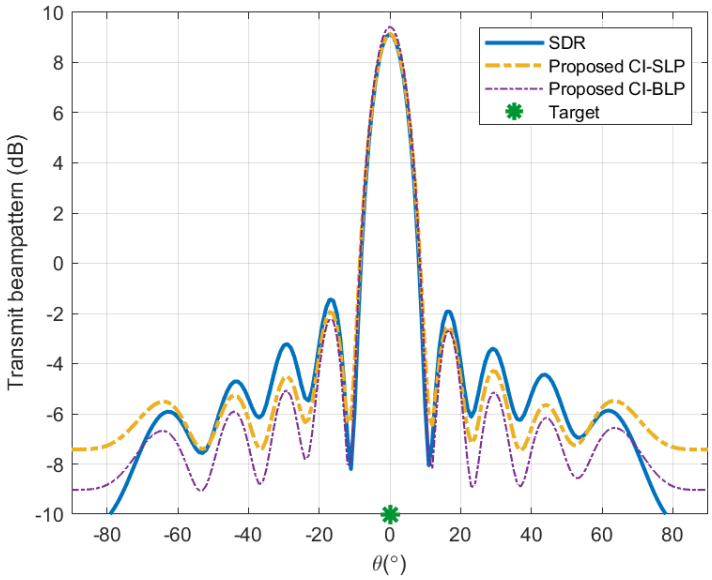

Fig. C Transmit beampatterns, $N = 10$, $K_{\mathrm{u}} = 3$, $K_{\mathrm{t}} = 1$, $\Gamma = 4\mathrm{dB}$, $p_0 = 30\mathrm{dB}$, 8PSK.

Compared with Fig. 3 and Fig. 5 in the paper, it can be seen that the higher modulation order leads to degraded SER performance for all ISAC precoding schemes, while the transmit beampatterns remain almost unchanged.

(2) **Reviewer:** *In Algorithm 1, the authors use the Hooke-Jeeves pattern search algorithm to solve the optimization problem in Equation (37). The authors should explain the reason for choosing the Hooke-Jeeves pattern search algorithm.*

Authors: Regarding the Reviewers' concern on the reason for choosing Hooke-Jeeves pattern search algorithm, firstly the purpose of choosing Hooke-Jeeves pattern search algorithm to solve the optimization problem in Eq. (37) is to reduce the computational complexity. The Hooke-Jeeves pattern search algorithm is an iterative derivative-free method. At each iteration, we first probe the vector $\boldsymbol{\mu}$ along each dimension with a fixed step size to detect the most favorable descent direction. If no further improvement can be achieved, the step size is halved. It can be observed that the optimization problem in Eq. (37) has extremely simple constraints, which allows it to be solved by the Hooke-Jeeves pattern search algorithm with markedly reduced

computational complexity.

In this revision, we have included the statement below Eq. (37) as follows:

"Note that the problem $\mathcal{P}_4^{\mathrm{TPC}}$ can be more efficiently solved than the problem $\mathcal{P}_3^{\mathrm{TPC}}$ via the Hooke-Jeeves pattern search algorithm [39]. The Hooke-Jeeves pattern search algorithm is an iterative derivative-free method. At each iteration, we first probe the vector $\boldsymbol{\mu}$ along each dimension with a fixed step size to detect the most favorable descent direction. If no further improvement can be achieved, the step size is halved. It can be observed that the problem $\mathcal{P}_4^{\mathrm{TPC}}$ has extremely simple constraints, which allows it to be solved by the Hooke-Jeeves pattern search algorithm with markedly reduced computational complexity. After solving the dual problem $\mathcal{P}_4^{\mathrm{TPC}}$, we can obtain $\boldsymbol{\mu}^*$ and then we can obtain $\tilde{\mathbf{x}}_{\mathrm{E}}^*$ of $\mathcal{P}_3^{\mathrm{TPC}}$ via (31)."

(3) **Reviewer:** *At the beginning of Section IV, the authors should provide some references to support the research on per-antenna power constraints.*

Authors: We thank the Reviewer for the valuable suggestion regarding the references. Most existing works on precoding consider the total power constraint, while in practical systems, each transmit antenna is usually equipped with its dedicated power amplifier. Therefore, it is more realistic to design precoding approaches that incorporate the per-antenna power constraint. In [R1], the authors investigate the conventional block-level precoding under the per-antenna power constraint in ISAC systems, while in [R2] and [R3], the authors focus on symbol-level precoding design under the per-antenna power constraint in communication-only systems.

In this revision, we have included the relevant references and added the following statement at the beginning of Section IV:

"In practical systems, each transmit antenna is usually equipped with its

dedicated power amplifier. Therefore, it is more realistic to design ISAC precoding approaches that incorporate the per-antenna power constraint [41]-[43]. In this section we design the transmit ISAC waveform matrix **X** under per-antenna power constraint."

[R1] F. Liu, L. Zhou, C. Masouros, A. Li, W. Luo, and A. Petropulu, "Toward Dual-functional Radar-Communication Systems: Optimal Waveform Design," IEEE Trans. Signal Process., vol. 66, no. 16, pp. 4264–4279, 2018.

[R2] Y. Wen, H. Wang, A. Li, X. Liao, and C. Masouros, "Low-Complexity Interference Exploitation MISO Precoding Under Per-Antenna Power Constraint," IEEE Trans. Wireless Commun., vol. 23, no. 8, pp. 9943–9957, 2024.

[R3] Y. Wen, J. Yang, A. Li, X. Liao, and C. Masouros, "Parallel Solution for Per-Antenna Power Constrained Symbol-Level MU-MISO Precoding," IEEE Trans. Commun., pp. 1–1, 2025.

(4) **Reviewer:** *In the description of Figure 1, the authors should add explanations for* $\mathrm{s}_k^{\mathrm{right}}$ *and* $\mathrm{s}_k^{\mathrm{left}}$.

Authors: We thank the Reviewer for the valuable suggestion on improving the readability of our paper. In Fig 1, $\mathrm{s}_k^{\mathrm{right}} = \overrightarrow{OC}$ and $\mathrm{s}_k^{\mathrm{left}} = \overrightarrow{OD}$, which represent the projections of the k-th user's nominal constellation point onto the two decision boundaries, respectively.

In this revision, we have updated the statement above Eq. (11) as follows:

"… To be more specific, in Fig. 1, $\overrightarrow{OA}$ can be decomposed along the two decision boundaries for QPSK modulation as $\overrightarrow{OA} = \overrightarrow{OC} + \overrightarrow{OD} = s_k^{\mathrm{right}}[l] + s_k^{\mathrm{left}}[l]$, where $s_k^{\mathrm{right}}[l]$ and $s_k^{\mathrm{left}}[l]$ represent the projections of the k-th user's nominal constellation point onto the two decision boundaries, respectively. In a similar way, the received signal $\overrightarrow{OB}$ can also be

decomposed as follows."

(5) **Reviewer:** *Using k as the iteration index variable in Algorithm 3 is confusing. Please explain and correct it if necessary.*

Authors: We thank the Reviewer for the careful reading of our paper. We apologize for our oversight and have updated Algorithm 3 in Section IV-D. In Algorithm 3, the iteration index is represented by the variable *loop* to avoid any confusion. In addition, we have updated Eq. (52), Eq. (53) and Eq. (54) accordingly.

(6) **Reviewer:** *In the simulation results, the authors are advised to adjust the font size in the figures to make the content clear.*

Authors: We thank the Reviewer for the careful reading of our paper. Following the Reviewer's suggestion, we have adjusted the font sizes in all the figures of Section V.